NASA CR-66428

FEASIBILITY STUDY OF A MINIATURE SOLID-STATE PRESSURE TRANSDUCER

C. D. Parker

Prepared for

National Aeronautics and Space Administration
Langley Research Center
Langley Station
Hampton, Virginia

Final Report

July 1967

(Prepared under Contract NAS1-6249 by the Solid State Laboratory of the Research Triangle Institute, Research Triangle Park, North Carolina.)

FOREWORD

This report was prepared by the Research Triangle Institute, Research Triangle Park, North Carolina, on NASA Contract NAS1-6249, "Feasibility Study of a Miniature Solid-State Pressure Transducer." This work was administered under the direction of the Flight Instrumentation Division at Langley Research Center by Mr. Charles A. Hardesty.

This study was performed by the Solid State Laboratory of the Research Triangle Institute under the general direction of Dr. R. M. Burger. Dr. J. J. Wortman was the Laboratory Supervisor and C. D. Parker was the Project Leader. Special credits are also due H. L. Honbarrier and P. P. Rasberry for their invaluable contribution in this investigation.

CONTENTS

LIST OF FIGURES

LIST OF FIGURES (continued)

LIST OF FIGURES (continued)

LIST OF TABLES

1.0 Introduction

The purpose of this study has been to investigate the feasibility of exploiting the piezojunction effect as the sensory phenomenon in a miniature solid state pressure transducer for possible application on meteorological sounding rockets and balloons. The piezojunction effect occurs at high stress levels in silicon ($\sigma > 10^9$ dynes/cm^2) and is characterized by an exponential increase in minority carrier density with increasing stress above the threshold stress level. The increased minority carrier density can be readily detected in the electrical characteristics of a p-n junction, and exponential increases in p-n junction current for a constant applied voltage result when the junction area is stressed above the threshold level. Theoretical considerations of the piezojunction phenomenon are reviewed in Section 2.0 of this report.

The exponential relationship that exists between minority carrier density in silicon and stress, and the ease of detecting changes in minority carrier density through the electrical characteristics of p-n junctions make the piezojunction phenomenon particularly attractive as a stress transducer. The phenomenon is further enhanced as a transducing mechanism by the small size of p-n junctions. A small force applied to a small area, for example, can result in a very large stress in the contact area. By causing changes in physical phenomena, e.g., pressure, acceleration, and force, to vary the force applied to the area of a p-n junction, a family of sensitive, piezojunction transducers can result. In Section 3.0 of this report, mechanical configurations that cause pressure variations to alter the stress or force applied to a p-n junction are discussed.

Two pressure transducer configurations are particularly attractive. One is a simple diaphragm configuration in which the diaphragm material

(silicon) is stressed directly by a pressure differential that balloons the diaphragm. This arrangement has many significant advantages derived from the absence of a physical contact to p-n junction area. Its principal disadvantage results from the fact that the piezojunction effect is less sensitive to a tensional stress than to a compressional stress. The second of these configurations is the silicon needle sensor in which the stress-sensitive p-n junction is formed at the apex of a silicon needle. Its advantages are the absence of any alignment problems, the p-n junction area can be very small and the entire area readily stressed. Its disadvantages are those associated with the physical contact to a second mechanical member of the transducer.

The fabrication of the silicon needle sensors and pressure transducers are described in Section 4.0 of this report. Stress-sensitive needle sensors and sensitive pressure transducers have been fabricated, and their characteristics are described herein. Pressure changes of 30 cm H_2O ($\approx$ 22 mm Hg), for example, have yielded greater than two orders-of-magnitude change in junction current at constant voltage.

2.0 Theoretical Considerations - A Summary

The piezojunction phenomenon in silicon is summarized in this section in the interest of completeness. A more complete theoretical discussion has been published by Wortman, et al., [Refs. 1, 2, 3].

2.1 Energy Band Considerations

The electrical characteristics of semiconductors and the piezojunction phenomenon are conveniently described in terms of the energy band structure. Silicon, as is the case for all semiconductors, has a forbidden energy region (energy gap) separating the valence energy levels (valence band) and the conduction energy levels (conduction band). In momentum space (k-space), the maximum valence levels in silicon occur at k = (000) and the minimum conduction levels occur in the <100> directions. The maximum valence levels, Γ'_{25}, are degenerate in energy with a separation resulting from the two angular momentum quantum numbers, j = 3/2 and j = 1/2. The j = 1/2 level is approximately 0.04 eV below the j = 3/2 and is neglected in the computations that follow in this section. The Γ'_{25} level is also degenerate at k = (000) and is slightly split for k $\neq$ (000) due to spin orbit coupling. The Γ'_{25} valence levels of silicon near k = (000) are illustrated for silicon in Fig. 1. The splitting of the Γ'_{25} (j = 3/2) level for k $\neq$ (000) causes the effective masses for the two levels to be different, and the upper and lower levels are frequently referred to as "heavy" holes and "light" holes, respectively.

When stress is applied to the silicon crystal, the Γ'_{25} (j = 3/2) energy levels become non-degenerate as illustrated in Fig. 2. E_{V1} and

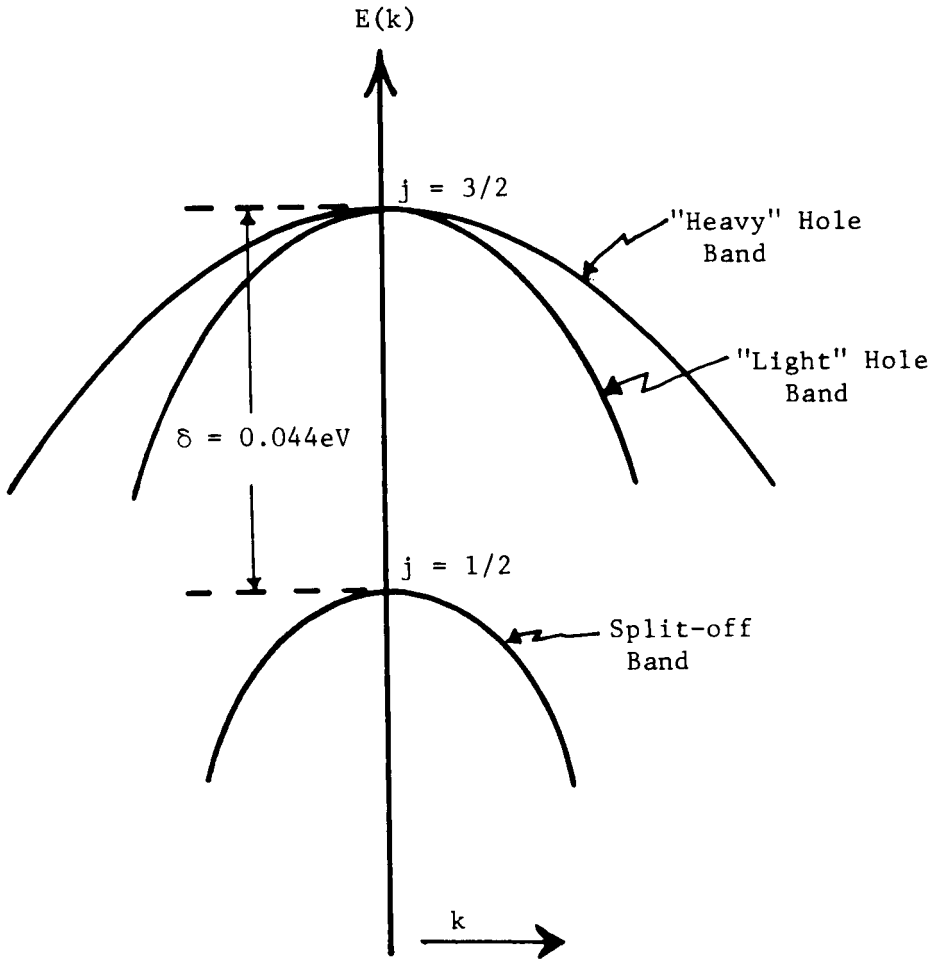

Fig. 1. The Valence Bands of Silicon Near $\bar{k} = 0$ [Ref. 4]

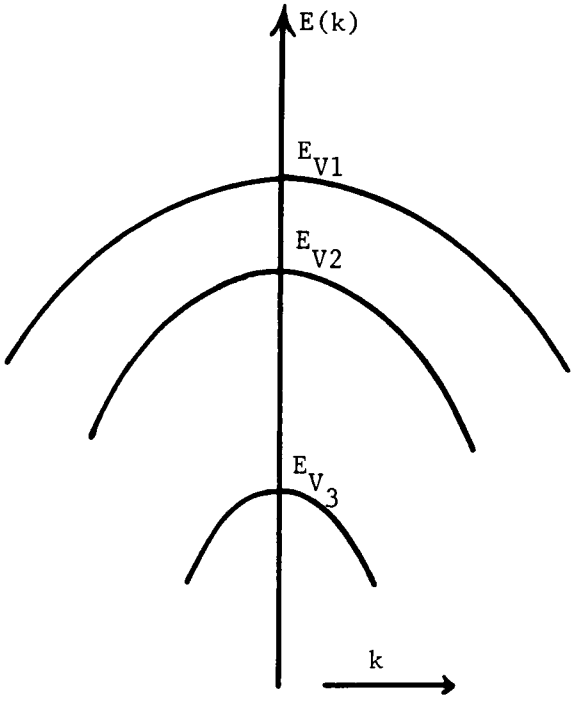

Fig. 2. The Split Valence Bands of Silicon for a Compressional Stress [Ref. 4]

E_{V2} are the Γ'_{25} (j = 3/2) "heavy" and "light" hole energy levels, and E_{V3} is the Γ'_{25} (j = 1/2) energy level. Since it is the width of the forbidden energy gap that is of interest, it is convenient to consider the change in the Γ'_{25} (j = 3/2) energy levels with strain. These are given by

$$\Delta E_{V1} = E_{V1} - E_o = D_d e + \{(\tfrac{2}{3} D_u)^2 (e_1^2 + e_2^2 + e_3^2 - e_1e_2 - e_1e_3 - e_2e_3) + \tfrac{1}{3} (D'_u)^2 (e_4^2 + e_5^2 + e_6^2)\}^{\frac{1}{2}}, \quad (1)$$

and

$$\Delta E_{V2} = E_{V2} - E_o = D_d e - \{(\tfrac{2}{3} D_u)^2 (e_1^2 + e_2^2 + e_3^2 - e_1e_2 - e_1e_3 - e_2e_3) + \tfrac{1}{3} (D'_u)^2 (e_4^2 + e_5^2 + e_6^2)\}^{\frac{1}{2}}, \quad (2)$$

where the D's are the deformation potential coefficients, and the e_i's are the components of strain (see Appendix A). More specifically, D_d is the energy level shift per unit dilation of the Γ'_{25} (j = 3/2) band edge, D_u is porportional to the splitting of the band edge induced by uniaxial shear strain along the [100] axis, and D'_u is proportional to the band edge splitting induced by uniaxial shear strain along the [111] axis. E_o is the unstrained Γ'_{25} (j = 3/2) energy level [Ref. 1].

Strain also induces changes in the conduction bands, and changes in the conduction band minima are of equal importance with changes in the

valence band maximum. Silicon has six conduction band minima located along the principal crystal axes. Since these minima change in pairs, i.e., since one cannot distinguish between the conduction band minima located along the [100] and [$\bar{1}$00] axes, only three conduction band minima need be considered, E_{C1}, E_{C2} and E_{C3}. Changes in these conduction band minima in the stress region of interest are given by [Ref. 1]

$$\begin{aligned} \Delta E_{C1} &= \Xi_d\, e + \Xi_u\, e_1 \,, \\ \Delta E_{C2} &= \Xi_d\, e + \Xi_u\, e_2 \,, \\ \Delta E_{C3} &= \Xi_d\, e + \Xi_u\, e_3 \,, \end{aligned} \tag{3}$$

where the Ξ's are the deformation potential coefficients, the e_i's are the engineering strain components along the crystal axes, (see Appendix A) and

$$e = e_1 + e_2 + e_3 \,. \tag{4}$$

Changes in the valence band and conduction band maxima and minima energy levels gives rise to a change in the carrier concentrations in the conduction band. In silicon, for example, the density of electrons associated with the six conduction band minima is given by

$$\begin{aligned} n = 2\left(\frac{2\pi kT}{h^2}\right)^{3/2} \{ & m_{C1}{}^{3/2} \exp\left[-\left(\frac{E_{C1} - E_F}{kT}\right)\right] + m_{C2}{}^{3/2} \exp\left[-\left(\frac{E_{C2} - E_F}{kT}\right)\right] \\ & + m_{C3}{}^{3/2} \exp\left[-\left(\frac{E_{C3} - E_F}{kT}\right)\right]\} \,, \end{aligned} \tag{5}$$

where E_F = the Fermi energy level, and

m_{C1} = the effective electron masses associated with the energy minima.

Eq. (5) can be rewritten as

$$n = \frac{n_o}{3} \exp\left(\frac{\Delta E_F}{kT}\right) \left[\exp\left(-\frac{\Delta E_{C1}}{kT}\right) + \exp\left(-\frac{\Delta E_{C2}}{kT}\right) + \exp\left(-\frac{\Delta E_{C3}}{kT}\right)\right] , \quad (6)$$

where n_o = unstressed electron density, and

ΔE_F = change in the Fermi level.

Similarly, the carrier concentration associated with the valence band maxima is given by

$$p = 2\left(\frac{2\pi kT}{h^2}\right)^{3/2} \left\{m_{V1}^{3/2} \exp\left[-\left(\frac{E_F - E_{V1}}{kT}\right)\right] + m_{V2}^{3/2} \exp\left[-\left(\frac{E_F - E_{V2}}{kT}\right)\right]\right\} \quad (7)$$

where m_{Vi} = effective masses associated with the valence band maxima, E_{Vi}. In Eq. 7, the Γ'_{25} (j = 1/2) energy level has been neglected. If the small difference between m_{V1} and m_{V2} is also neglected a good approximation for silicon, Eq. (7) can be written as

$$p = \frac{p_o}{2} \exp\left(-\frac{\Delta E_F}{kT}\right) \left[\exp\left(\frac{\Delta E_{V1}}{kT}\right) + \exp\left(\frac{\Delta E_{V2}}{kT}\right)\right] , \quad (8)$$

where p_o = the hole concentration with no stress.

The $\exp\left(-\frac{\Delta E_F}{kT}\right)$ terms in Eqs. (6) and (8) can be evaluated by setting the majority carrier density equal to the impurity density and assuming the ionization energy to be independent of stress. Consequently, the hole density remains constant in p-type material, for example, and

$$\exp\left(\frac{\Delta E_F}{kT}\right) = \frac{1}{2} \left[\exp\left(\frac{\Delta E_{V1}}{kT}\right) + \exp\left(\frac{\Delta E_{V2}}{kT}\right)\right] . \quad (9)$$

Substituting Eq. (9) into (6) yields the ratio of stressed to unstressed minority carrier density, $\gamma_v(e)$, in the p-type material as [Ref. 1]

$$\gamma_\nu(e) = \frac{n_p}{n_{po}} = \frac{1}{6}\left[\exp\left(\frac{\Delta E_{V1}}{kT}\right) + \exp\left(\frac{\Delta E_{V2}}{kT}\right)\right]\left[\exp\left(-\frac{\Delta E_{C1}}{kT}\right) + \exp\left(-\frac{\Delta E_{C2}}{kT}\right)\right.$$

$$\left. + \exp\left(-\frac{\Delta E_{C3}}{kT}\right)\right] . \tag{10}$$

Following a similar procedure for n-type material, it can be shown that [Ref. 1]

$$\frac{p_n}{p_{no}} = \frac{n_p}{n_{po}} = \gamma_\nu(e) . \tag{11}$$

2.2 Deformation Potential Coefficients

The deformation potential coefficients have been evaluated both theoretically and experimentally, and the values used herein are underlined in Table I. It is possible that the deformation potential coefficients change with doping. In particular, the value D_u' is considerably uncertain, and $\gamma_\nu(e)$ has been calculated using two different values of D_u'. The value of D_u' which should be used is not known; however, it is probably between 2.68 and 10. The value of 2.68 appears from experimental observations to be a better value.

2.3 Calculated Values of $\gamma_\nu(e)$

The ratio of stressed to unstressed minority carrier density, $\gamma_\nu(e)$, has been caluclated for hydrostatic and uniaxial [100], [011] and [111] tensional and compressional stresses. Figs. 3 and 4 are plots of $\gamma_\nu(e)$ as a function of compressional and tensional stresses, respectively, for $D_u' = 2.68$. Figs. 5 and 6 are similar plots for $D_u' = 10$. For a hydrostatic and uniaxial [100] stress, $\gamma_\nu(e)$ is independent of D_u'. The exponential

Table I. [Ref. 3]

Deformation Potential Coefficients (eV/unit dilation) for Si. (Kleinman's Theoretical Values are Shown in Brackets. Values Used in This Investigation are Underlined.)

Coefficient	Si
D_d	[- 2.09]
D_u	2.04,[a] [3.74]
D'_u	2.68,[a] 10,[e] [4.23]
Ξ_d	[- 4.99]
Ξ_u	11,[b] 8.3,[c] [+ 9.6]
$D_d - (\Xi_d + \frac{1}{3}\Xi_u)$	- 1.44,[d] [- 0.30]

a J. C. Hensel and G. Feher, Phys. Rev. 129, 1041 (1963).

b D. K. Wilson and G. Feher, Phys. Rev. 124, 1968 (1961).

c J. E. Aubrey, W. Gubler, T. Henningsen, and S. H. Koenig, Phys. Rev. 130, 1667 (1963).

d W. Paul, J. Phys. Chem. Solids 8, 196 (1959).

e J. J. Wortman, Private Communication.

increase in $\gamma_\nu(e)$ with stress in a basic characteristic of the piezojunction phenomenon. It is evident from Figs. 3 through 6 and $\gamma_\nu(e)$ is most sensitive to a [100] compressional stress, and least sensitive to a [111] tensional stress. It is also evident that the piezojunction effect

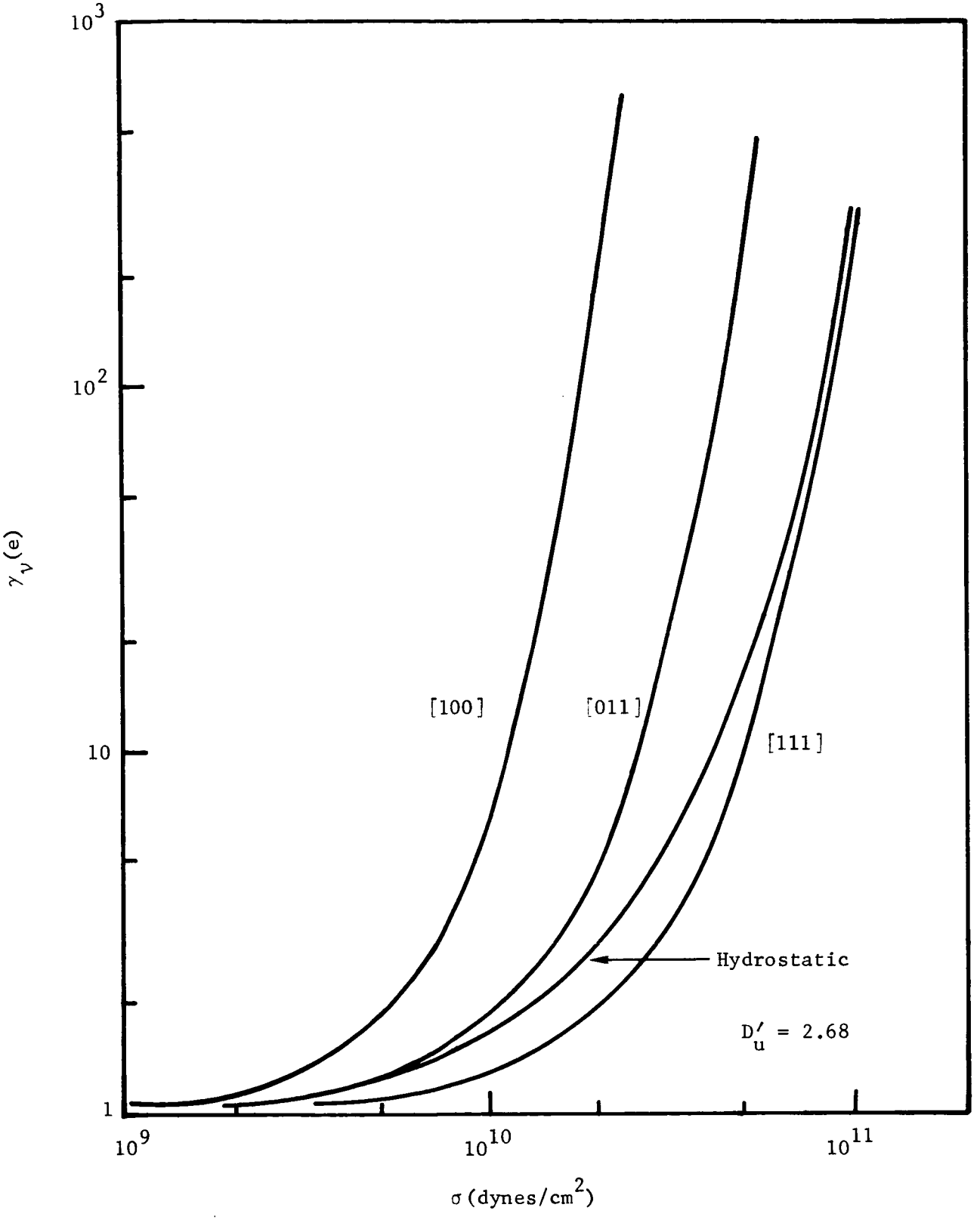

Fig. 3. Ratio of Stressed to Unstressed Minority Carrier Density for a Hydrostatic, [100], [011] and [111] Uniaxial, Compressional Stress

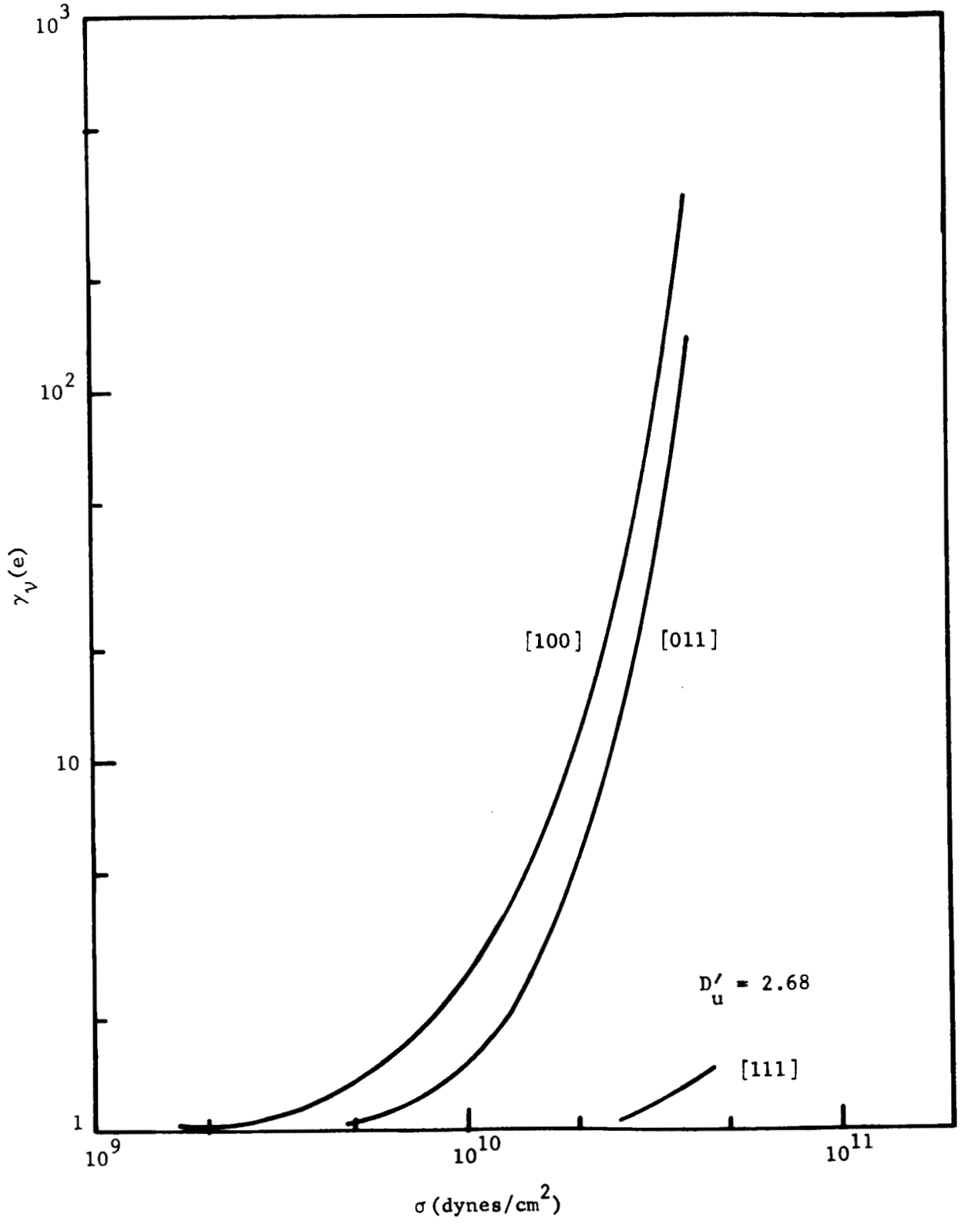

Fig. 4. Ratio of Stressed to Unstressed Minority Carrier Density for a [100], [011] and [111] Uniaxial, Tensional Stress

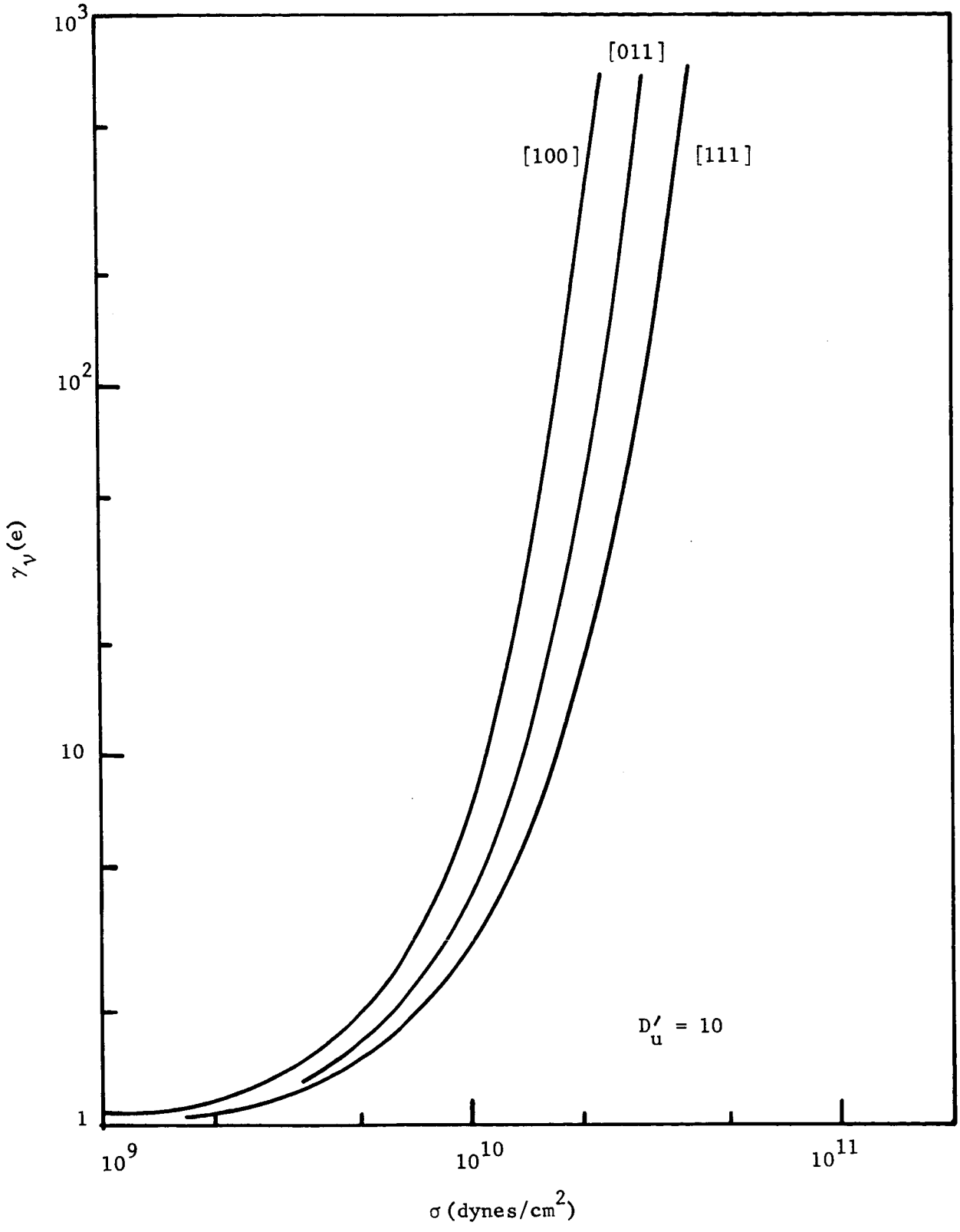

Fig. 5. Ratio of Stressed to Unstressed Minority Carrier Density for a [100], [011] and [111] Uniaxial, Compressional Stress

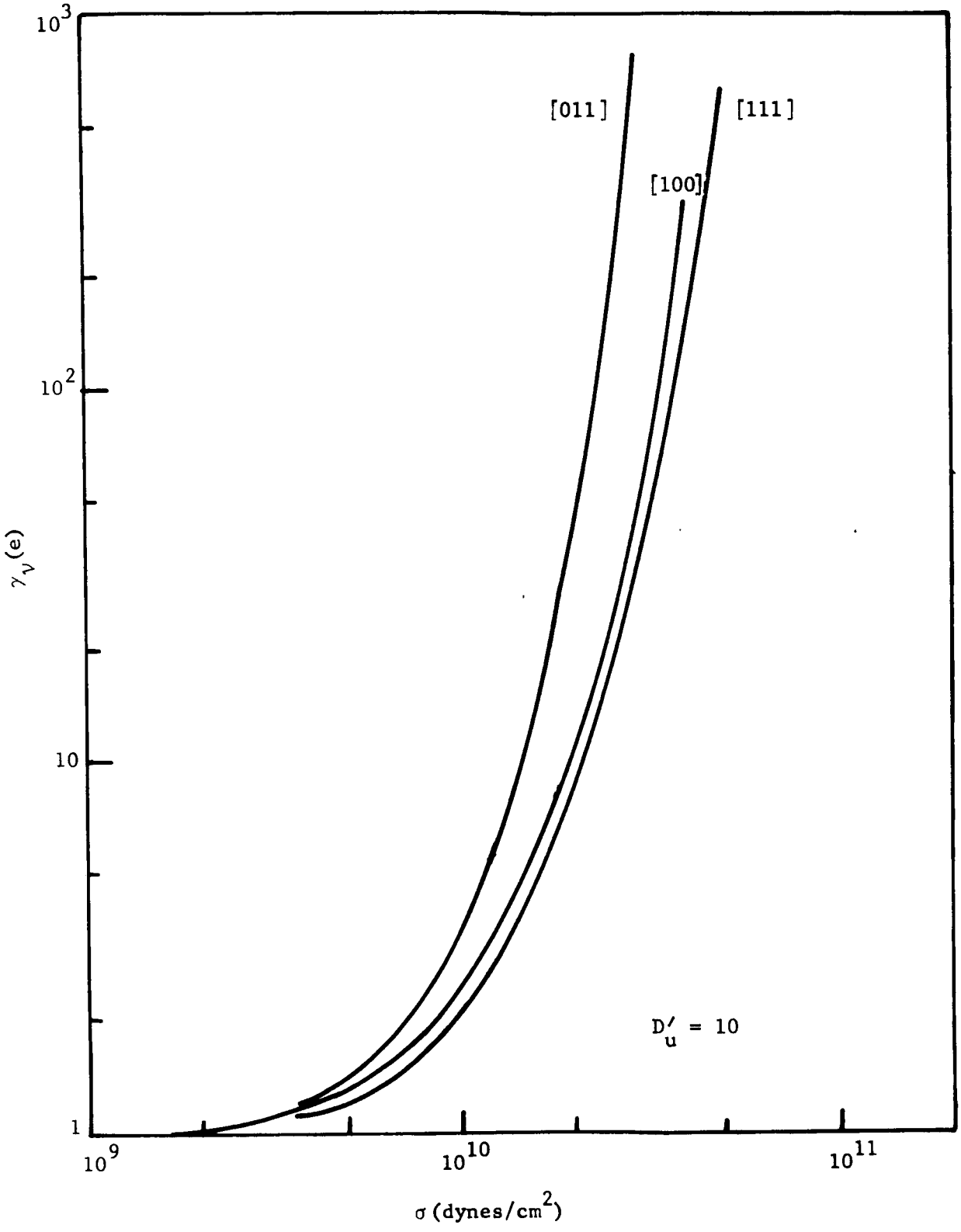

Fig. 6. Ratio of Stressed to Unstressed Minority Carrier Density for a [100], [011] and [111] Uniaxial, Tensional Stress.

is significant at stress levels greater than 10^9 dynes/cm^2, i.e., order-of-magnitude changes occur in $\gamma_\nu(e)$ with changes in stress. The mechanical strength of silicon limits the stress that can be applied to a p-n junction in silicon and is the basic limitation to changes that can be achieved in $\gamma_\nu(e)$. The fracture strength of silicon varies from sample to sample and depends to a large extent on the surface conditions [Ref. 5]. However, order of magnitude changes have been experimentally observed in $\gamma_\nu(e)$.

2.4 Effect of Stress on p-n Junction Characteristics

The effect of stress on p-n junction characteristics has been described by Wortman, et al., in terms of $\gamma_\nu(e)$. Changes in other parameters are assumed to be negligible as compared with the exponential change of $\gamma_\nu(e)$ with stress above 10^9 dynes/cm^2. This model also neglects the contribution of surface generation-recombination currents.

The total current (I_T) in p-n junctions is the sum of the ideal current (I_I) and the generation-recombination currents (I_R).

$$I_T = I_I + I_R \ . \tag{12}$$

For forward biased conditions, the bulk generation-recombination current is given approximately by

$$I_R = \frac{a\ \gamma_\nu(e)\ [\exp(qV/kT)-1]}{1 + b\sqrt{\gamma_\nu(e)}\ \exp(qV/kT)} \ , \tag{13}$$

and the ideal current is given by

$$I_I = C\ \gamma_\nu(e)\ [\exp(qV/kT)-1] \ , \tag{14}$$

such that Eq. (12) becomes [Ref. 2]

$$I_T = \frac{a\,\gamma_\nu(e)\ [\exp(qV/kT)-1]}{1 + b\sqrt{\gamma_\nu(e)}\ \exp(qV/2kT)} + C\,\gamma_\nu(e)\ [\exp(qV/kT)-1]\ . \qquad (15)$$

The effect of stressing only a part of the total junction area is accounted for by considering that the total diode consists of two diodes in parallel, i.e., (1) a stressed diode, and (2) an unstressed diode. If the total area is A, for example, and the stressed area is A_s, then Eq. (14) becomes

$$I_I = \left[\frac{(A - A_s)}{A} + \frac{A_s}{A}\,\gamma_\nu(e)\right]\ [\exp(qV/kT)-1]\ . \qquad (16)$$

It is of interest here to consider the p-n junction current under different bias conditions. For large forward biases, Eq. (15) is approximately

$$I_T \simeq \frac{a}{b}\,(\gamma_\nu(e))^{\frac{1}{2}}\ \exp(qV/2kT) + C\,\gamma_\nu(e)\ \exp(qV/kT)\ . \qquad (17)$$

It is significant that for large forward biases, i.e., $V > 0.3$ volts, p-n junction current will have a larger dependence on the ideal component of current than the generation-recombination component. In experiments with mesa diodes, the forward-bias characteristics have been dominated by the generation-recombination (qV/2kT) current at voltages less than a few tenths of a volt, and by the ideal (qV/kT) current at higher voltages. For reverse-bias conditions the ideal current is much less than the generation-recombination current. The effects of stress onthe generation-recombination current in the reverse-biased mode is not easily described. Experimentally, reverse-biased p-n junctions have been observed to be very sensitive to stress

and relatively independent of voltage for voltages less than the breakdown voltage. The forward-biased characteristics, as shown in Eq. (17), is dependent upon $\gamma_{\upsilon}(e)$ and the applied voltage. Both stressed and unstressed p-n junction V-I characteristics are illustrated in the oscillogram of Fig. 7. This junction was formed in the point of a silicon needle

Hauser and Wortman [Ref. 3] have also investigated the effect of mechanical stress on the breakdown voltage of p-n junctions and, in the case of silicon, found the change in breakdown voltage to be

$$\frac{\Delta V}{V_B} \approx - \ (10^{-12} \ \text{cm}^2/\text{dyne}) \ \sigma \qquad (18)$$

where σ is the applied stress, ΔV is the change in breakdown voltage and V_B is the unstressed breakdown voltage. The change in breakdown

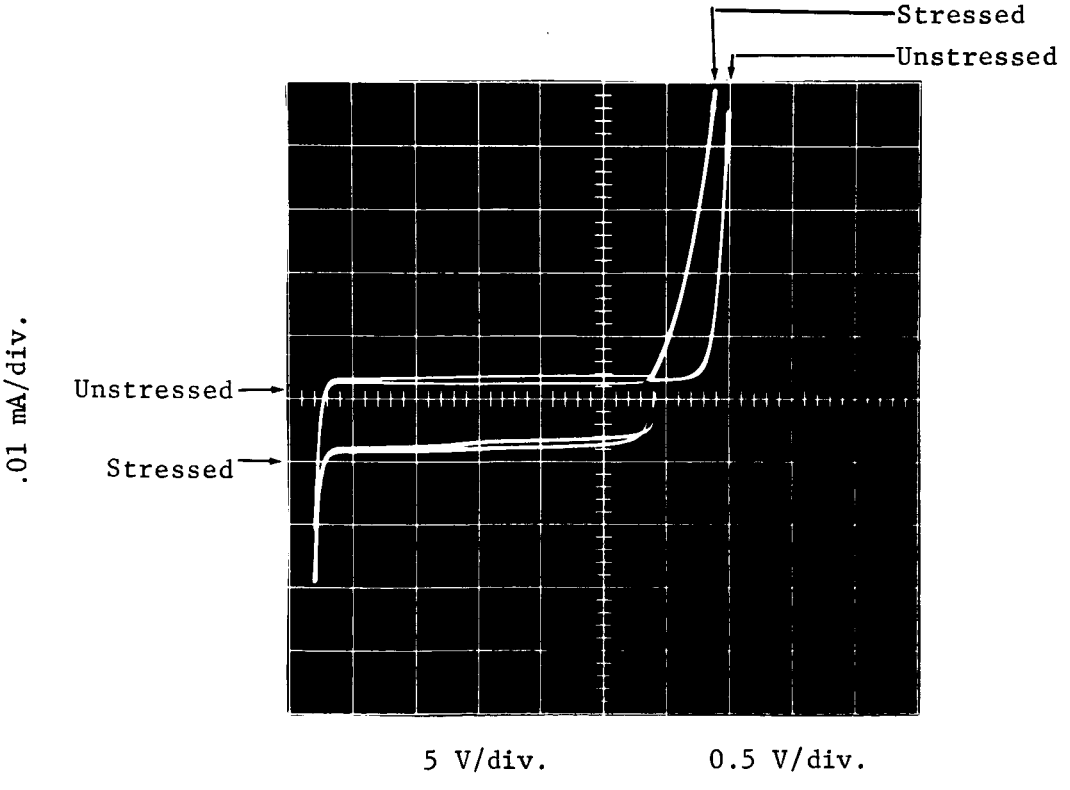

Fig. 7. Stressed and Unstressed V-I Characteristics of a p-n Junction (Silicon Needle Diode)

voltage is also independent of orientation. Since the breakdown voltage is a linear function of stress whereas the junction current at a voltage less than breakdown voltage is an exponential function of stress, the latter mode of operation is potentially a more sensitive transducing mechanism. However, if voltage is held constant across the device in the breakdown region, current can change greatly with small voltage changes. Breakdown voltage is also less sensitive to temperature changes than junction currents, and this mode of operation may have advantages in some applications.

The effects of stress on more complex silicon p-n junction structures is also of interest. Wortman, et al., has investigated the effects of stress upon transistor characteristics and p-n-p-n switches [Ref. 1]. If both sides of the emitter-base junction are stressed, the base and collector currents are changed several orders of magnitude for small changes in stress above 10^{10} dynes/cm^2. The current gain will not be affected if both junctions are similarly stressed. If only the emitter side of the junction is stressed ($e_e \gg e_b$) the base current increases orders of magnitude with stress while the collector current remains unchanged. Consequently, gain is reduced by stressing the emitter side of the base-emitter junction. If only the base side of the junction is stressed ($e_e \ll e_b$), the base and collector currents remain approximately the same.

The effect of stress on p-n-p-n diodes has also been investigated and concluded to be a complex function of numerous variables, e.g., the uniformity and location of the applied stress. The switching voltage

can increase or decrease with an increasing stress depending upon these various factors. The changes in switching voltage with stress can be very large, however, and the four-layer configuration is a promising transducer configuration.

3.0 Pressure Transducer Configurations

The piezojunction phenomenon, i.e., the sensitivity of p-n junction characteristics to stress, is a promising transducing mechanism. Since stress is force per unit area and the area of a p-n junction is characteristically very small, a relatively small force can bias a p-n junction in the sensitive region above 10^9 dyne/cm^2. In this region small changes in the applied force, i.e., applied stress, will cause large changes in the p-n junction characteristics. If a constant voltage is applied to a diode mechanically biased in the piezojunction region, order-of-magnitude changes in the diode current will occur with small changes in the applied stress. In the preceding section of this report, the ratio of stressed to unstressed minority carrier density ($\gamma_v(e)$) was shown to be an exponential function of stress, and the forward and reverse currents a linear function of $\gamma_v(e)$.

The purpose of this research was to determine the feasibility of exploiting the piezojunction effect as the transducing mechanism for a pressure sensor. The following paragraphs describe several pressure transducer configurations in which pressure variations are caused to vary the stress applied to a p-n junction.

3.1 The Simple Diaphragm Configuration

The simple diaphragm configuration illustrated in Fig. 8 has several advantages, and considerable efforts were invested in fabricating pressure transducers with this configuration. In Fig. 8, a silicon diaphragm with a diffused p-n junction is stressed in a bending mode by a pressure differential across the diaphragm. If the diaphragm is thin a pressure

differential can cause a relatively large deflection, i.e., greater than one-half the diaphragm thickness, such that the entire diaphragm material will be stressed, i.e., there will be no middle plane of zero stress. Under these conditions it is common for the silicon diaphragm to withstand greater stress levels without fracturing than a thicker plate withstands. The principal advantages of the simple diaphragm configuration are (1) that large area stresses are achieved, (2) the mechanical simplicity that eliminates much opportunity for mechanical creep, misalignment and hysteresis, (3) the elimination of the electrical contact problems that plague many other configurations, and (4) the elimination of mechanical contacts that can cause damage to the p-n junction area. The advantages of eliminating mechanical contacts for creating stresses cannot be overstated. On a microscopic level, the mechanical interface between an indenter point, for example, and a p-n junction cannot be described, but it is very probably that a microscopic

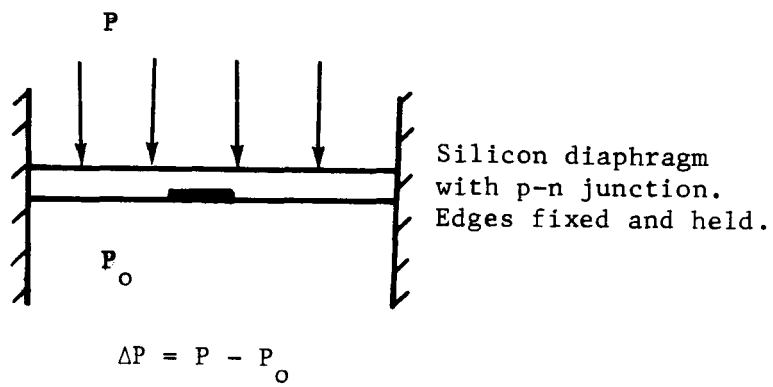

Fig. 8. The Simple Diaphragm Pressure Transducer

area of the junction will be damaged by stress before a significant portion of the junction area is stressed. Physical damage may take the form of dislocations, for example, which may change the electrical properties of the junction. Dislocations and other defects acts as generation-recombination centers which are semipermanent in nature and contribute a hysteresis effect.

Hysteresis has been observed in practically all observations of the piezojunction effect. A notable exception is the experimental observations of Wortman and Wooten [Ref. 6]. These authors applied a large-area, uniaxial, compressional stress to silicon planar p-n junctions by bonding the silicon chip to spring steel and bending the assembly. Under these circumstances, the piezojunction effect was observed without hysteresis up to some critical stress level. Beyond this critical level, the epoxy adhesive creeped and resulted in a hysteresis effect.

Roark [Ref. 7] has tabulated formulas relating diaphragm stresses and pressure differentials to deflection for several configurations similar to Fig. 8. These have been evaluated in order to assess the suitability of the simple diaphragm configuration as a pressure transducer. Consider, for example, that the diaphragm edges are fixed and held as illustrated in Fig. 8. The relationship between the differential pressure and maximum diaphragm stress (center stress) can be determined from the following equations [Ref. 7]:

$$\frac{(\Delta P)a^4}{Et^4} = \frac{16}{3(1-\nu^2)}\left[\left(\frac{y}{t}\right) + 0.488\left(\frac{y}{t}\right)^3\right], \text{ and} \qquad (19)$$

$$\sigma_{max} = 2.86\ E\left(\frac{yt}{a^2}\right) + 0.976\ E\left(\frac{y}{a}\right)^2 , \qquad (20)$$

where

t = diaphragm thickness,

a = diaphragm radius,

ΔP = pressure differential,

E = Young's Modulus,

ν = Poisson's ratio,

y = maximum (center) deflection, and

σ_{max} = maximum diaphragm stress.

Equations (19) and (20) have been evaluated with the following parameter values, for example:

$t = 2.5 \times 10^{-3}$ in.,

$a = 0.28$ in.,

$E = 1.69 \times 10^{12}$ dynes/cm^2, and

$\nu = 0.35$,

and the results are shown in Fig. 9. The significant factors from Fig. 9 are (1) the large pressure differential required to stress the diaphragm material to the 10^9 - 10^{10} dynes/cm^2 region, (2) the relatively large deflections, and (3) the "sensitivity" of stress to pressure changes. (In the low-stress region, $\Delta\sigma/\Delta P \approx 7.7 \times 10^5$ dynes/cm^2/torr, and in the high-stress region, $\Delta\sigma/\Delta P = 3.4 \times 10^5$ dynes/cm^2/torr.)

In order to function as a pressure transducer, the simple diaphragm configuration would require a significant pressure bias. The sensitivity of diaphragm stress to pressure differential changes is also low. For

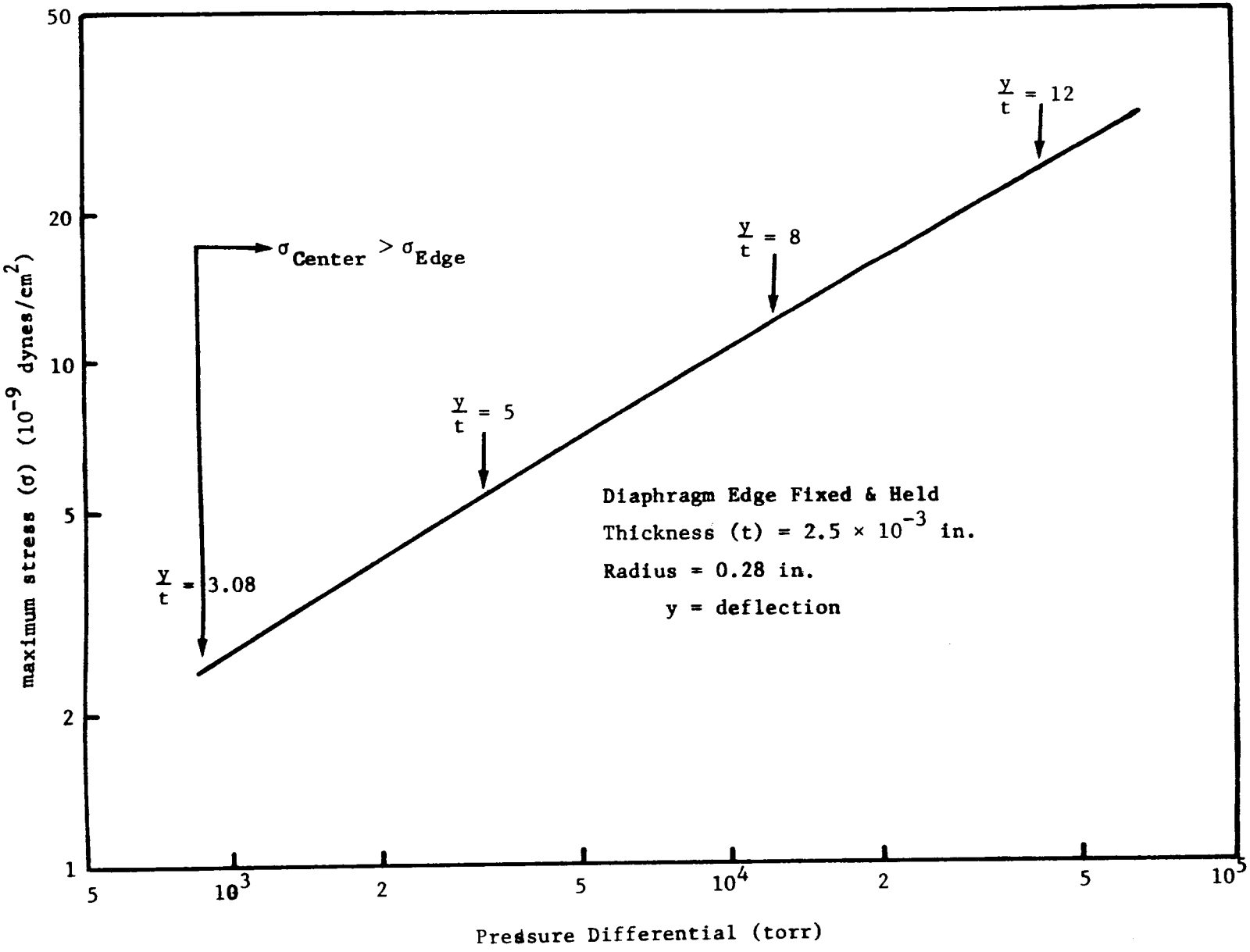

Fig. 9. Maximum Stress in a Simple Diaphragm Versus Pressure

the illustrative example presented herein, a pressure change of one atmosphere will yield a change in stress of 0.6×10^9 dynes/cm^2 and, consequently, a very small change in $\gamma_\nu(e)$. The simple diaphragm configuration is further compromised in that the resulting maximum diaphragm stress is a tensional stress rather than compressional. A comparison of Figs. 3 and 4, for example, shows the compressional stress to be a more desirable mode of operation. Since $\gamma_\nu(e)$ is significantly greater for a given compressional stress above 10^9 dynes/cm^2 than for a tensional stress.

There is little advantage to be gained by changing the parameters of the simple diaphragm configuration. Increasing the radius (a) and/or reducing the thickness (T) provides for reaching a given stress level with less pressure differential. The 2.5×10^{-3} in. diaphragm is approximately as thin as can be practically processed, however, and increasing the radius increases the liklihood of crystal fracture due to imperfections. There is also a limit to the radius of available silicon ingots, i.e., approximately 3/4 in.

Irrespective of the problems associated with the simple diaphragm, e.g., a tensional rather than a compressional stress and the requirement of a relatively large pressure bias, the many advantages were such as to warrant an experimental investigation. Numerous diaphragms were fabricated with p-n junctions and stressed in test jigs similar to the illustration of Fig. 8. For example, the diaphragm edge was fixed and held (approximately) in some experiments, and simply supported in others.

In all of these experiments, diaphragm rupture occurred without the piezojunction effect being observed.

3.2 The Indenter Configuration

A modification of the simple diaphragm configuration is the indenter point or stress concentrating pin arrangement illustrated in Fig. 10. The p-n junction may be either on the top surface or on the bottom surface as illustrated in Fig. 10. In either case, the stress profile is a complex function of position along the diaphragm surface. The purpose of this configuration is to concentrate the stress in a selective area on the silicon surface. Experimentally, the piezojunction effect has been observed with the indenter in direct contact with the junction. It has not been observed with other arrangements, e.g., with the p-n junction diffused into the opposite, no-contact side of the diaphragm.

With the indenter point located in the center of the diaphragm as illustrated in Fig. 10, the force on the indenter for a given pressure differential across the diaphragm is approximately [see Appendix B]

$$F = F_o + \frac{\Delta P \pi a^2}{4} , \tag{21}$$

where

F_o = bias force when $P = 0$,

ΔP = Pressure differential across diaphragm, and

a = diaphragm radius.

The force on the indenter is balanced by an equal and opposite force on the diaphragm area in contact with the indenter. The stress applied to the diaphragm by the indenter point is a function of the force, F in Eq. (21), and the area of the indenter-diaphragm contact.

The stress on silicon needle point as a function of force has been derived by Wortman [Ref. 8] assuming the configuration illustrated in

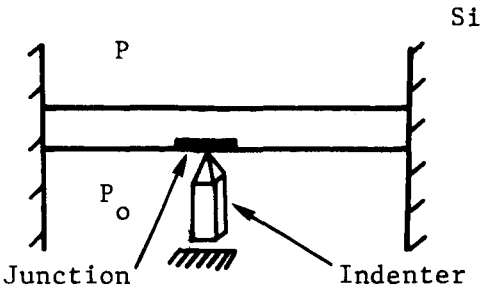

Fig. 10. The Indenter Point Pressure Transducer Configuration

Fig. 11 with circular symmetry. Although this analysis assumes an inflexible base, it should be a good approximation for a flexible diaphragm base and its inverse, i.e., the indenter configuration. Wortman gave the maximum stress as

$$\sigma_{max} = \frac{3F}{2\pi r^2} \text{ , where} \tag{22}$$

$$r = \text{radius of the contact area} = \left(3/2 \text{ RF } \frac{(1-\nu^2)}{E}\right)^{1/3} . \tag{23}$$

Therefore,

$$\sigma_{max} = kF^{1/3} . \tag{24}$$

The average stress is [Ref. 8]

$$\sigma_{avg} = \frac{F}{\pi r^2} = 2/3 \, \sigma_{max} . \tag{25}$$

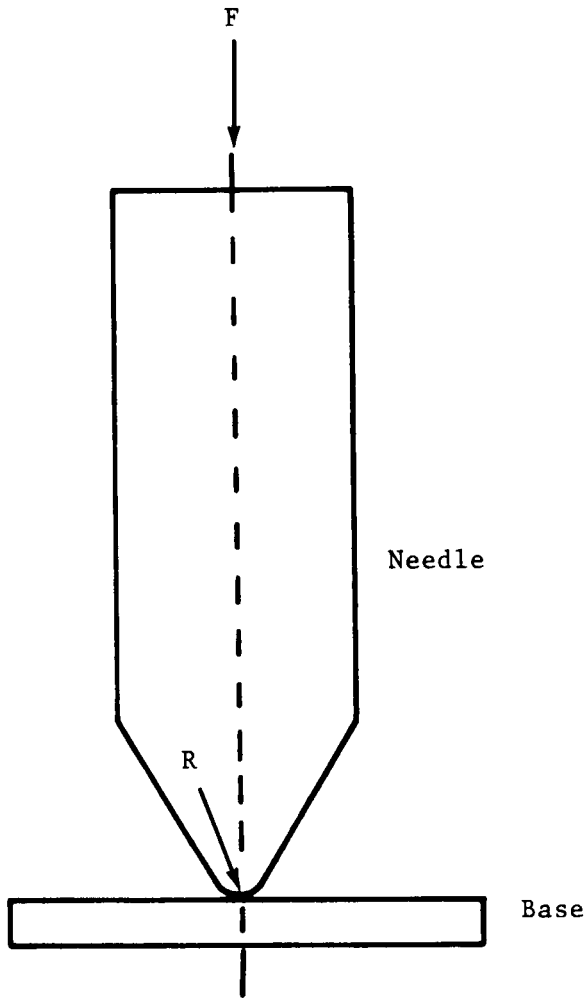

Fig. 11. An Illustration of a Needle Stressed Against a Base Material

Eqs. (21) and (24) can be combined to estimate the change in stress, for example, for a change in differential pressure across the diaphragm;

$$\Delta\sigma_{max} = k\Delta P^{1/3} \quad . \tag{26}$$

In practice, k in Eq. (26) is difficult to evaluate and is probably not a constant.

The piezojunction effect has been observed in several adaptations of the indenter point configuration. In Fig. 12, for example, a mesa diode is stressed by an "indenter point", and a typical result is plotted in Fig. 13 where the forward current is caused to change by four orders of magnitude [Ref. 4].

A commerical piezojunction pressure transducer has been marketed that utilizes an indenter point to apply stress to a planar transistor. Some typical specifications for this unit are [Ref. 9]:

Sensitivity $\approx$ 4 volts/14 in.H_2O ,

Linearity $\approx$ 0.5%, and

Hysteresis $\approx$ 0.5% .

The indenter point has several disadvantages. The liklihood and results of silicon surface damage as a result of indenter point contact was discussed in the preceding section. Alignment problems during fabrication are also difficult to overcome.

In the event of misalignment, it is likely that only a small portion of the total junction area will be stressed and the piezojunction sensitivity significantly compromised (see Eq. 16). Most indenter point pressure

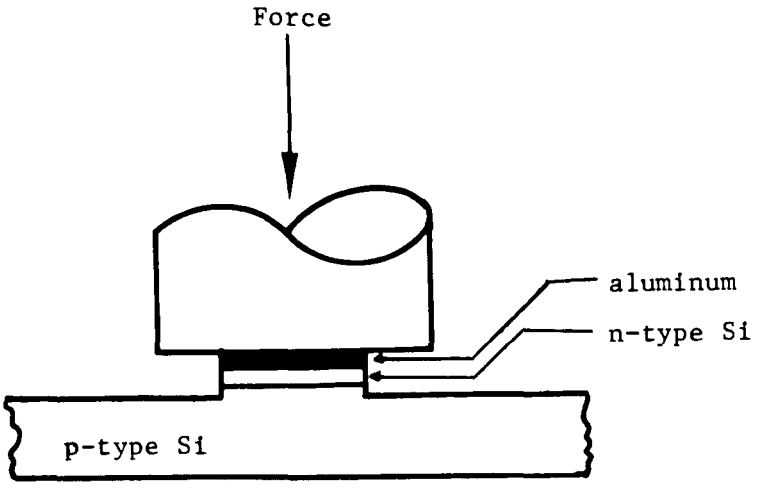

Fig. 12. An Illustration of a Mesa Diode Structure under Stress [Ref. 4]

transducer configurations also provide much opportunity for mechanical creep.

3.3 Silicon Needle Diode Configuration

An inverse of the indenter point configuration with several unique advantages is the silicon needle diode (silicon needle sensor). This arrangement, in which a p-n junction is fabricated at the tip of a silicon needle, is the most promising pressure transducer configuration investigated. As a pressure transducer, the needle sensor is compromised by a hysteresis effect and unreliable electrical contact to the p or n areas of the junction. However, these difficulties are characteristic of all configurations except the simple diaphragm which doesn't work. Hysteresis and electrical contacts in the needle sensor configuration

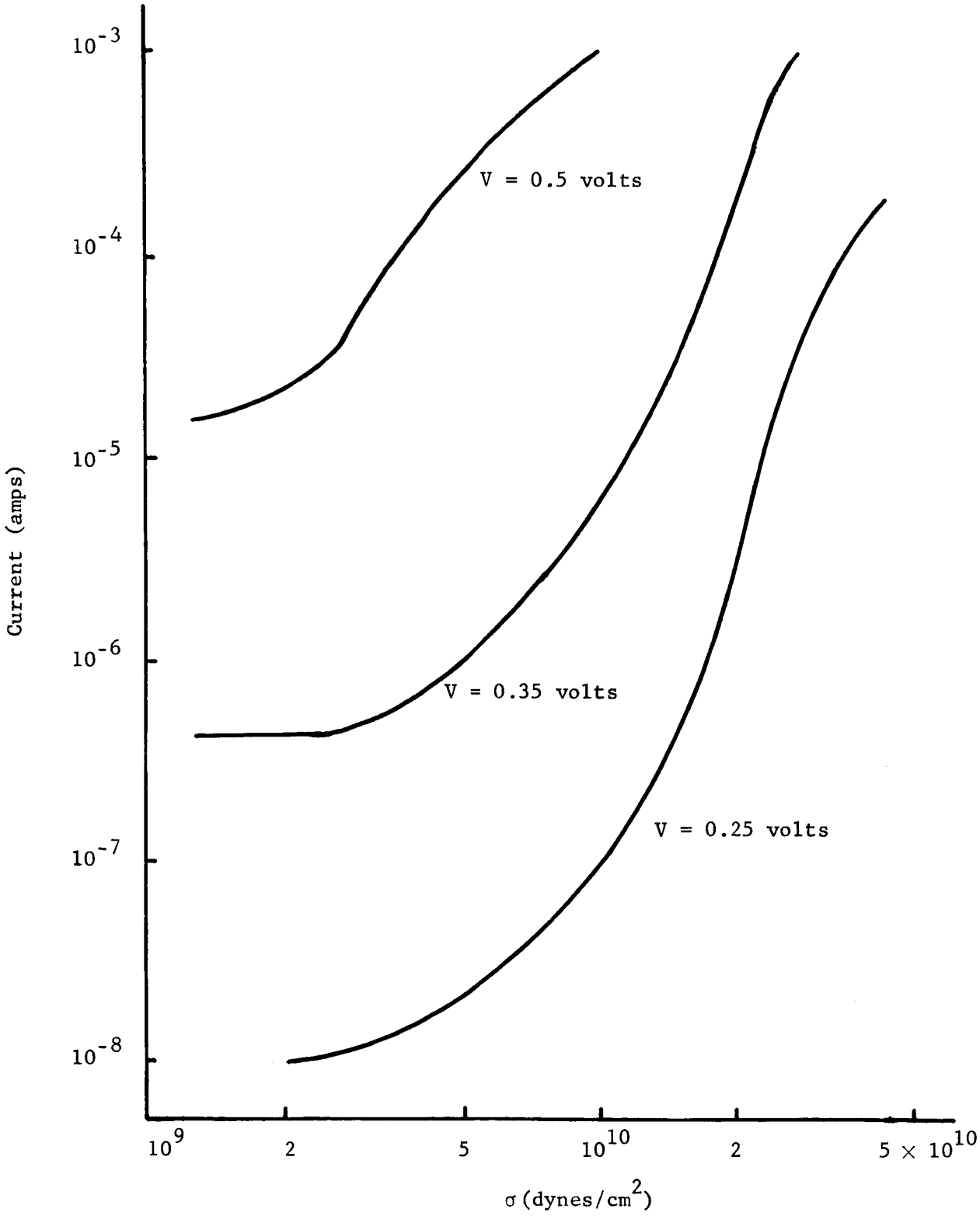

Fig. 13. Forward Current as a Function of Stress at Several Voltage Levels for a Mesa Diode [Ref. 4]

can be made at least as negligible as in other configurations. In addition, the needle sensors can have extremely small junctions, contact alignment problems are eliminated and the entire junction area tends to be stressed when the needle tip is forced against a diaphragm, for example. The needle sensors fabricated during this study have been sensitive to stress and durable and stable through rough laboratory handling.

The basic structure of the silicon needle sensor is illustrated in Fig. 14, and its application in a pressure transducer is illustrated in Fig. 15. An n-type silicon needle sensor is prepared, for example, protected with a thermally grown oxide which is selectively removed at the needle tip, and a p-type area is diffused into the tip. The junction thus created is very small and very near the surface of the tip, e.g., 0.5 μ deep. When the needle is forced against a smooth, hard surface, the junction is subjected to a high stress and the piezojunction effect is observed. The diode V-I characteristics shown in Fig. 7 (see Sec. 2.4) are from a silicon needle sensor.

The silicon needle sensors have been fabricated by applying planar device technology to the needle structure. Stress sensitive diodes resulted, and sensitive pressure transducers were fabricated with the needle sensors. All of the fabricational problems have not been solved, and the resulting diodes are not equal in quality to the better planar structures. When configurations more complex than the basic structures of Fig. 14 are fabricated, for example, fabricational difficulties become a basic limitation. During the latter part of this research, considerable

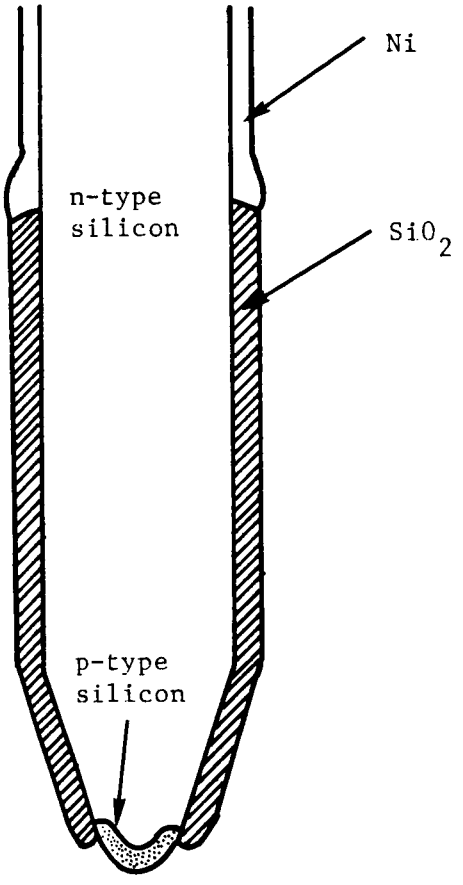

Fig. 14. Schematic of a Silicon Needle Sensor

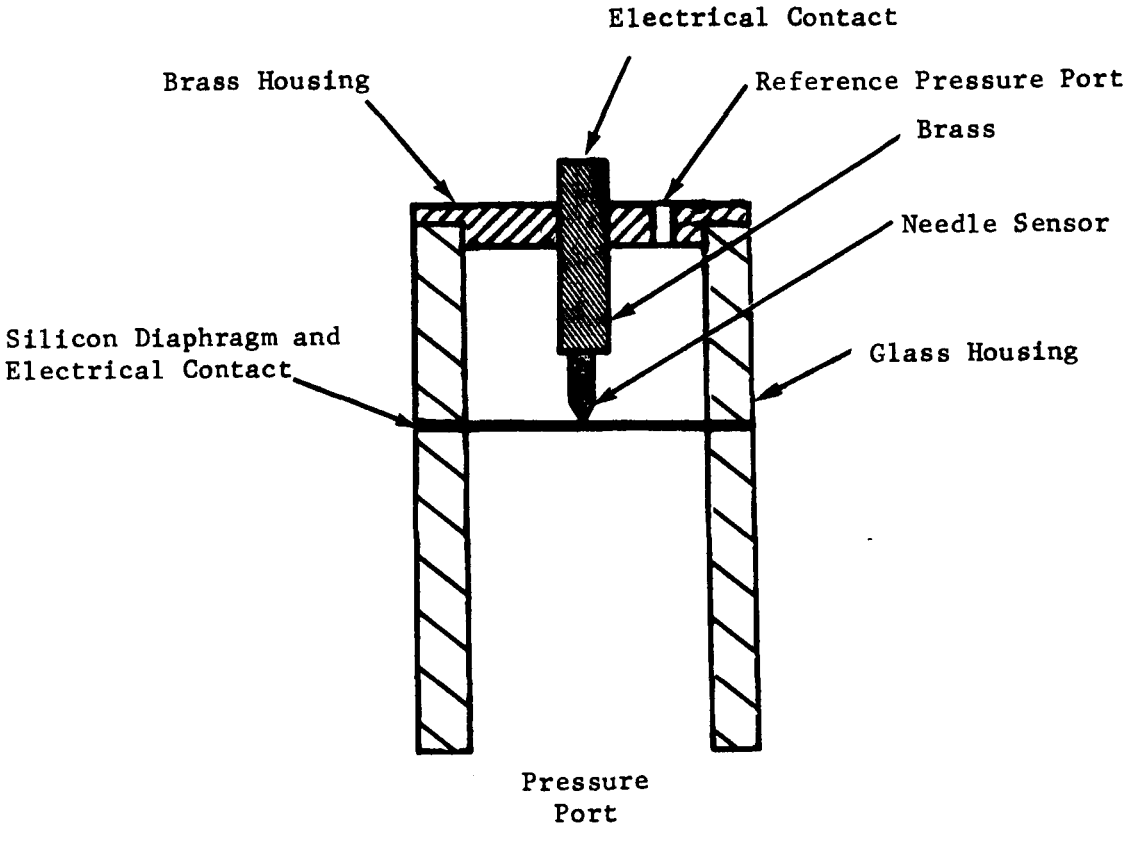

Fig. 15. Silicon Needle Sensor-Silicon Diaphragm Pressure Transducer.

effort was invested in improving the silicon needle fabrication technology and significant improvements were accomplished. Additional efforts are warranted in this area.

Because of the significant success of the silicon needle approach to fabricating pressure transducers, a complete section of this report (Sec. 4) is devoted to the silicon needle sensor.

3.4 Transistor and 4-Layer Switch Configurations

The problem of fabricating multiple p-n junctions in the apex of a silicon needle is complex. This problem not only requires the processing steps needed to fabricate diodes but also adds additional steps. The process is much simplified for multijunctions in which contact is needed only to the substrate (needle shank) and the outer junction. One example of this is a p-n-p-n or four-layer switch in which the gate junction is left open (no contact). In two junction devices (transistors) it is necessary that electrical contact be made to each of the doped regions if any useful electrical element is to be realized.

The requirements that each junction must exhibit are well known for multijunction devices. It is, therefore, a matter of translating present processing techniques with some modifications to the needle problem. For example, it will be necessary to mask certain areas on the apex of the needle with a high degree of precision.

The present study has been primarily concerned with the single junction fabrication problem in silicon needles. This problem is discussed in detail in a later section. It was felt that the diode problem must be solved before investigations of multijunction structures were

continued. It should be pointed out, however, that if space is not at a premium, it is better to stress only a diode. The nonlinear response of the diode to stress can easily be used in some complex, discrete component system to give the desired output. Stressing multijunction devices increases nonlinearity in the response and, in addition, may increase hysteresis. Generation-recombination current, for example, can be reduced to a negligible amount in a forward biased diode. Since it is this current that is primarily susceptable to hysteresis effects, a transistor of the same quality as the diode would be influenced to a larger extent since minority carriers must diffuse across the base region. It is likely that simple diodes will be more attractive as the sensor and certainly will be less expensive to manufacture.

4.0 The Silicon Needle Sensor

4.1 Needle Fabrication from Wafers

Silicon needle sensors were initially fabricated from square rods of silicon that were cut from commercial 1 Ω-cm. silicon wafers. Since it is important that the starting rods (blanks) have a square cross-section, the thickness of the starting wafer determines the blank dimensions. These were typically 3/8 inches long and 20 mils on each side. A conical needle tip is formed by electro-chemically etching one end of the starting blank. Non-square blanks result in wedge shaped tips with poor mechanical-strength characteristics.

The stress achieved by pressing a needle against a flat surface tends to be more isotropic than anisotropic and, therefore, the crystal orientation of the starting wafers is not critical. Good results were achieved by cutting 45° from the $\langle\bar{1}10\rangle$ direction in [111] wafers. (The direction numbers are $\left\langle \frac{-3 \pm \sqrt{7}}{2}, \frac{-1 \pm \sqrt{7}}{2}, \frac{-4 \pm \sqrt{7}}{2} \right\rangle$).

The starting blanks are thoroughly cleaned by processing through the procedure outlined below [Ref. 8]:

(1) Ultrasonically clean in TCE for 2 minutes.

(2) Rinse in TCE.

(3) Clean in Acetone for 5 - 10 minutes.

(4) Rinse in de-ionized water.

(5) Dry on filter paper.

(6) Plate in $CuSO_4$, HF solution for 5 minutes.

(7) Rinse two times in de-ionized water.

(8) Rinse in HNO_3 (70%) 3 times.

(9) Rinse in de-ionized water.

(10) Boil in 30% H_2O_2 for 10 minutes.

(11) Rinse in de-ionized H_2O.

(12) Ultrasonically clean in de-ionized H_2O 5 minutes.

(13) Rinse 3 times in de-ionized H_2O.

(14) Rinse in Acetone 2 - 4 minutes.

(15) Dry on filter paper.

(16) Rinse in HNO_3 at 50° C.

A clean needle blank is essential to the etching procedure described in the following paragraph.

A conically shaped point is etched on the needle blank by cycling the blank in and out of an etch solution composed of concentrated HNO_3 and concentrated HF. An ac potential is maintained between the blank and an electrode in the etch solution. The composition of the etch solution, the dip rate in and out of the etch, the current flow in the circuit, and the etch time are the parameters that control the etch results. Wortman made a study of the effects of varying these parameters and selected the following parameters as optimum [Ref. 8]:

(1) An etch solution of approximately 4.7 parts HNO_3 to 1 part HF,

(2) An RMS current (during the contact portion of the cycle) of approximately 50 mA,

(3) A dip rate greater than 20 cycles per minute,

(4) An etch time of approximately 4 minutes.

These parameter values produced consistently good results. Figure 16 is a photograph of the etching apparatus.

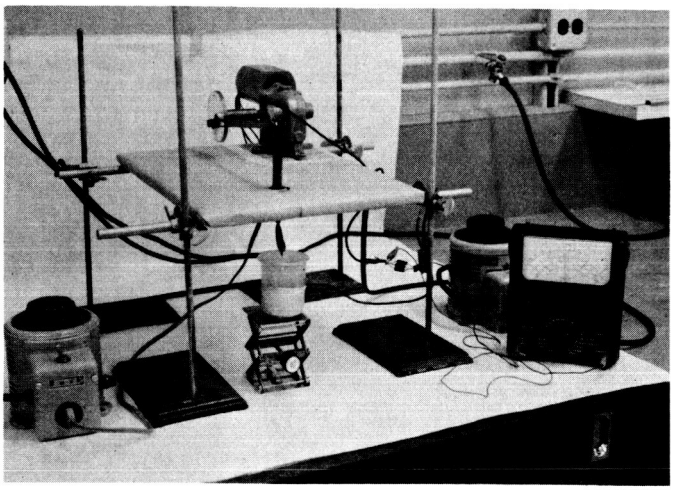

Fig. 16. Photograph of the Needle Etching Apparatus

Typical needle points are shown in Figs. 17 and 18. The scale in these photo-micrographs is 0.025 mm ($\approx$ 1 mil) per division. Generally speaking, the blunt points were mechanically stronger. It seems logical that the sharper points would have smaller junction areas and be more sensitive to an applied force. However, it appears that the size of the junction is not controlled closely with present processing techniques and, consequently, no positive correlation can be made between needle sharpness and sensitivity except in the extreme cases.

Once the silicon needles are prepared, p-n junctions are formed at the needle tips using techniques adapted from silicon planar technology. Silicon dioxide (SiO_2) is thermally grown over the entire needle surface and then selectively removed from the needle tip. The oxidation procedure is typically a dry-wet-dry procedure timed to yield approximately a 4000 Å oxide. The oxide-protected needle is coated with a commercial photoresist, e.g., KTFR, which is exposed and developed. During exposure, the tip of

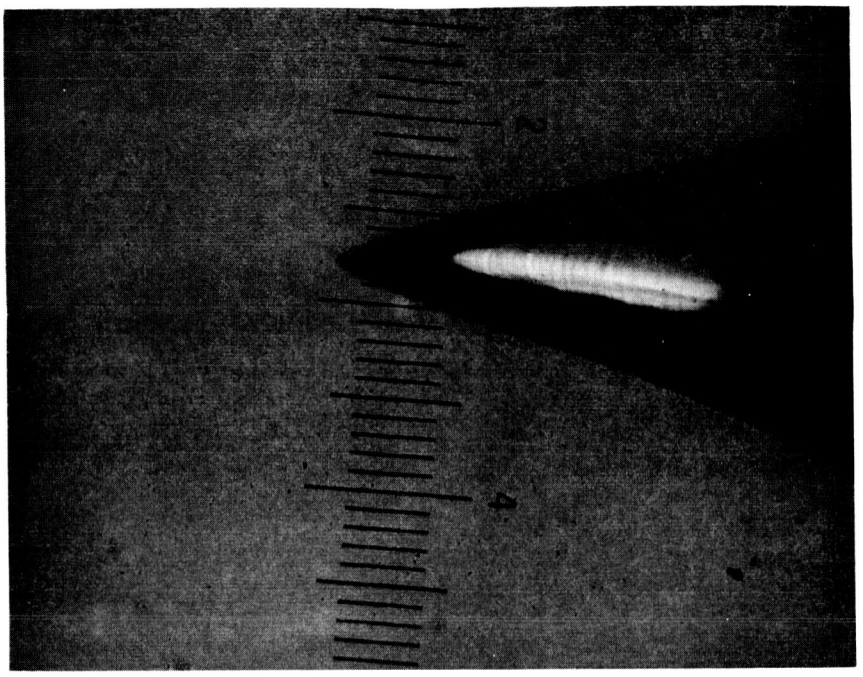

Fig. 17. Photo-micrograph of a Typical Needle Sensor Point (Scale: 0.025 mm/div.)

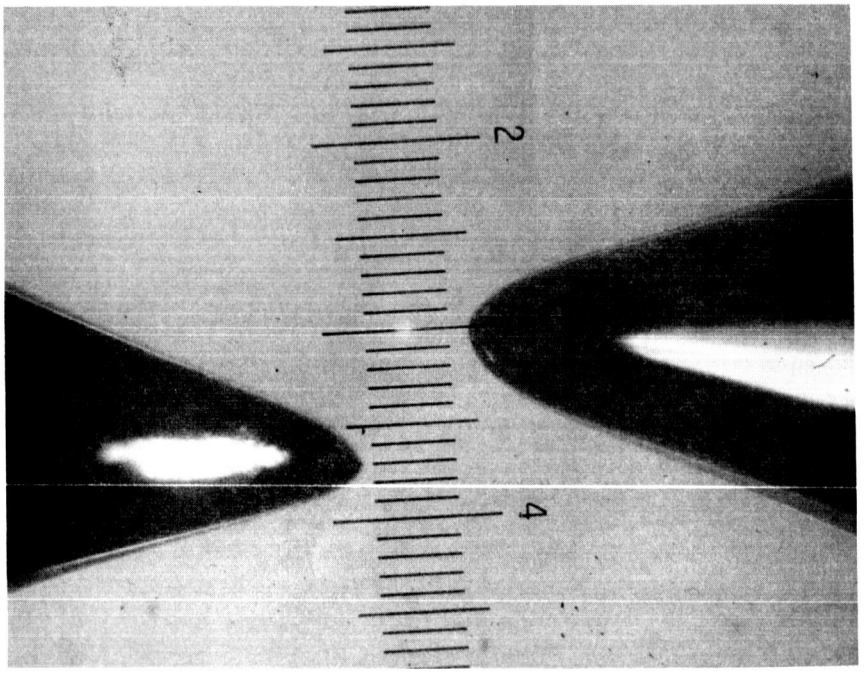

Fig. 18. Photo-micrograph of a Typical Needle Sensor Point (Scale: 0.025 mm/div.)

the needle is protected by carefully pressing the needle against a spring-loaded black metal plate. After exposure, the photoresist is developed exposing the SiO_2 at the tip of the needle. The exposed SiO_2 is etched in HF, creating a window at the needle tip. A p-n junction is then formed at the needle tip by removing the photoresist and placing the needle into a p-type (boron) diffusion furnace. Diffusion parameters have been controlled to yield shallow junctions and high surface concentrations. Typical junction parameters are 0.5 micron depths with a p-region resistivity of 150 ohms per square, and 1.3 micron depths with a p-region resistivity of 50 ohms per square. Stress sensitive p-n junctions with excellent electrical characteristics can be consistently fabricated using these procedures.

4.1.1 Experimental Results

Silicon needles have been fabricated with a wide range of sensitivities and V-I characteristics. One example is illustrated in Fig. 7. The V-I characteristics of Fig. 19 are more typical, however; i.e., the reverse characteristics are sensitive to voltage and stress. A dc plot of the force-reverse current characteristics for a typical needle diode is shown in Fig. 20. (The abscissa, force, is related to stress approximately as shown by Eq. 24. However, the radius of contact is unknown.) These characteristics are compromised by several factors. Data at stress levels lower than those on the graph are not repeatable because of the unreliable contact between the needle point and the material it is stressed against, and at high current levels resistance in the system tends to mask the piezojunction effect. The

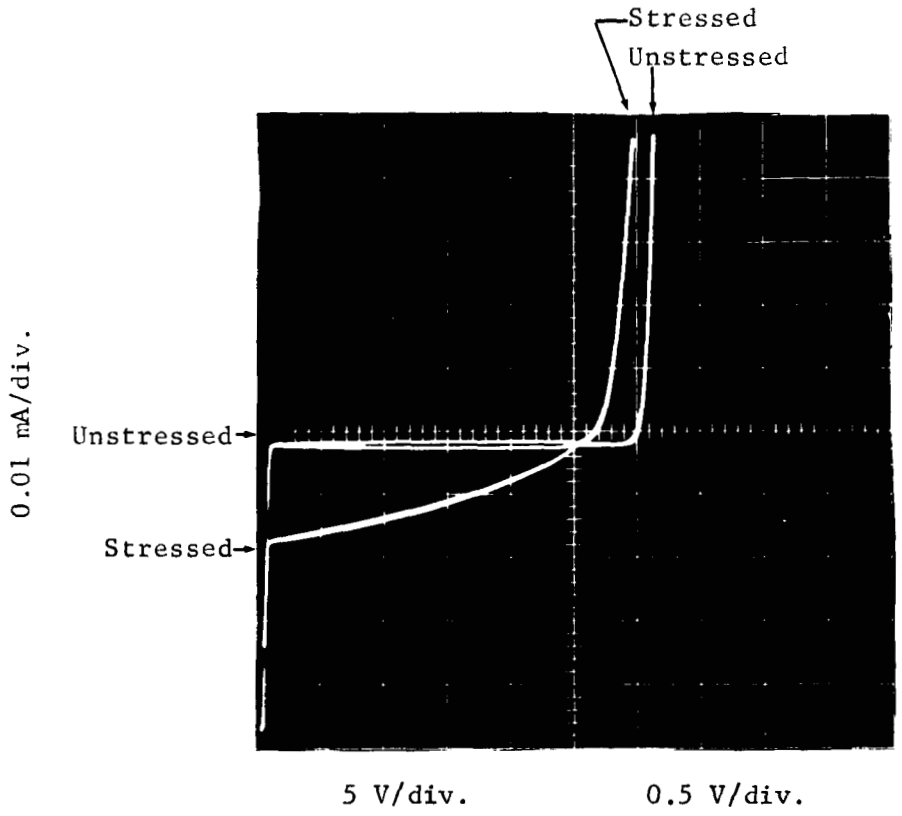

Fig. 19. Typical Stressed and Unstressed V-I Characteristics for a Silicon Needle Sensor

sensitivity of the needle illustrated in Fig. 20 is impressive, however; if this needle were stressed in the pressure transducer of Fig. 15 with the diaphragm diameter approximately one-quarter inch, for example, the total abscissa in Fig. 20 would correspond to approximately 25 mm Hg. Laboratory models of pressure transducers have approximated this sensitivity (see Sec. 4.2).

In both the forward and reverse directions, the V-I characteristics at constant stress and high current levels, e.g., $>10^{-4}$ amps, are approximately linear indicating that resistive elements are controlling the circuit characteristics. At low stress levels, the electrical contact between the needle tip and the surface it is stressed against is erratic

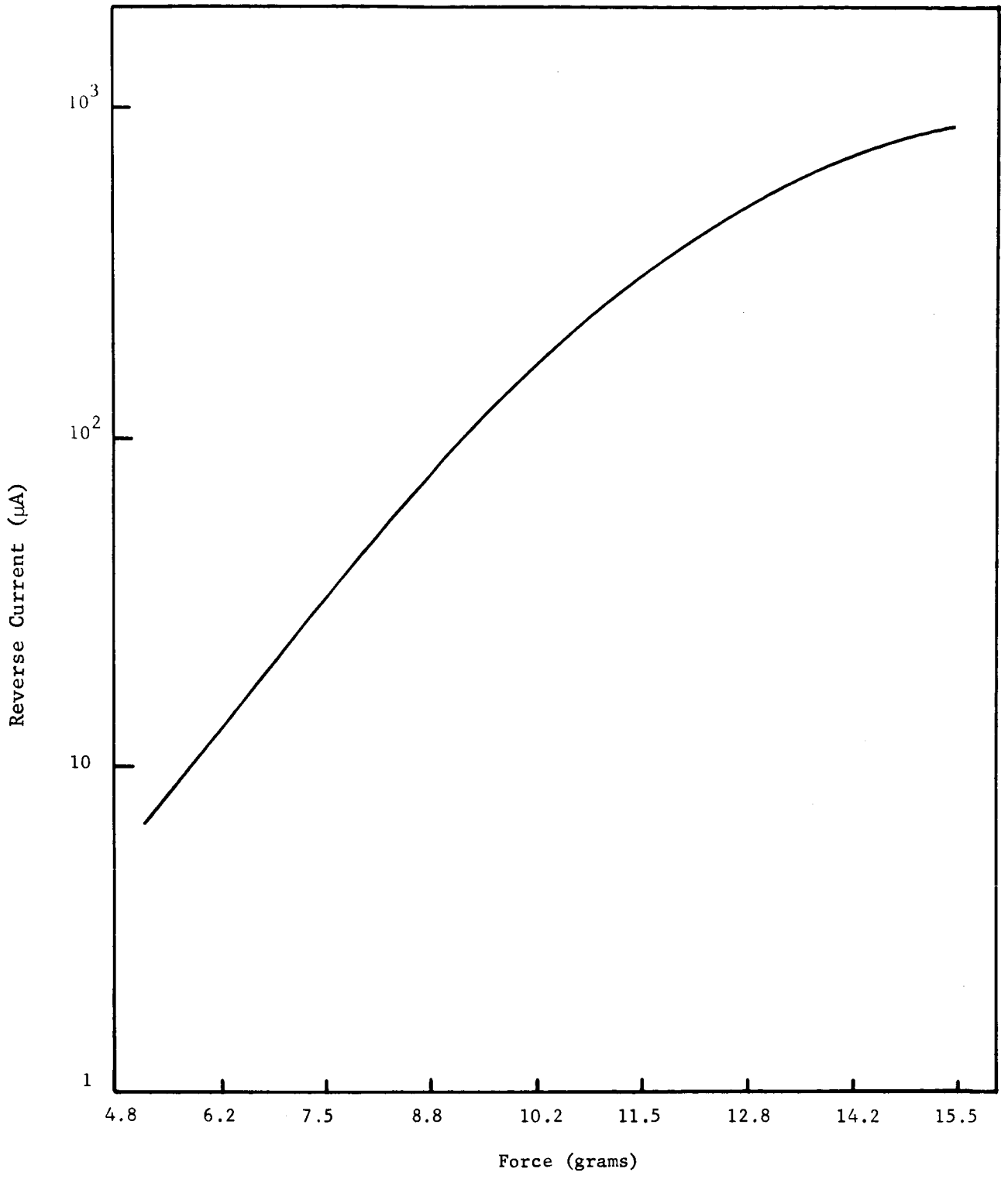

Fig. 20. Reverse Current Versus Stress in a Silicon Needle Sensor

and reliable experimental observations cannot be made. In the optimum stress-current region, a significant hysteresis effect consistently occurs. This hysteresis effect is illustrated in Fig. 21 where the force (stress)-current characteristics of a needle sensor stressed against gold-coated quartz are recorded for several cycles. The curves for each cycle fell within the dashed lines of Fig. 21. This hysteresis effect is approximately + 5%. The total hysteresis results from mechanical contributions as well as the actual contribution of the needle sensors. In the pressure transducer configuration where the mechanical contributions are more limited, the hysteresis effects are significantly less (see Sec. 4.2).

The sensitivity of the silicon needle as a stress sensor is also influenced by the material against which it is stressed (stress-plate). To increase sensitivity and reduce the hysteresis contributed by the mechanical characteristics of the stress-plate, it is desirable that the stress-plate material be stiffer than silicon, i.e., have a greater value of Young's modulus, and yield at a greater stress than does silicon. Few materials meet these requirements. Some examples are alumina, tungsten, beryllium oxide and quartz. The additional requirement that the surface of the stress-plate material be electrically conductive has limited the evaluation of stress-plate materials to stainless steel, silicon and quartz. Unless otherwise stated, all silicon needles discussed in this report were stressed against silicon. Fig. 22 illustrates the stress-current relationship in a single silicon needle stressed against stainless steel and silicon. The sensitivity is greater in the

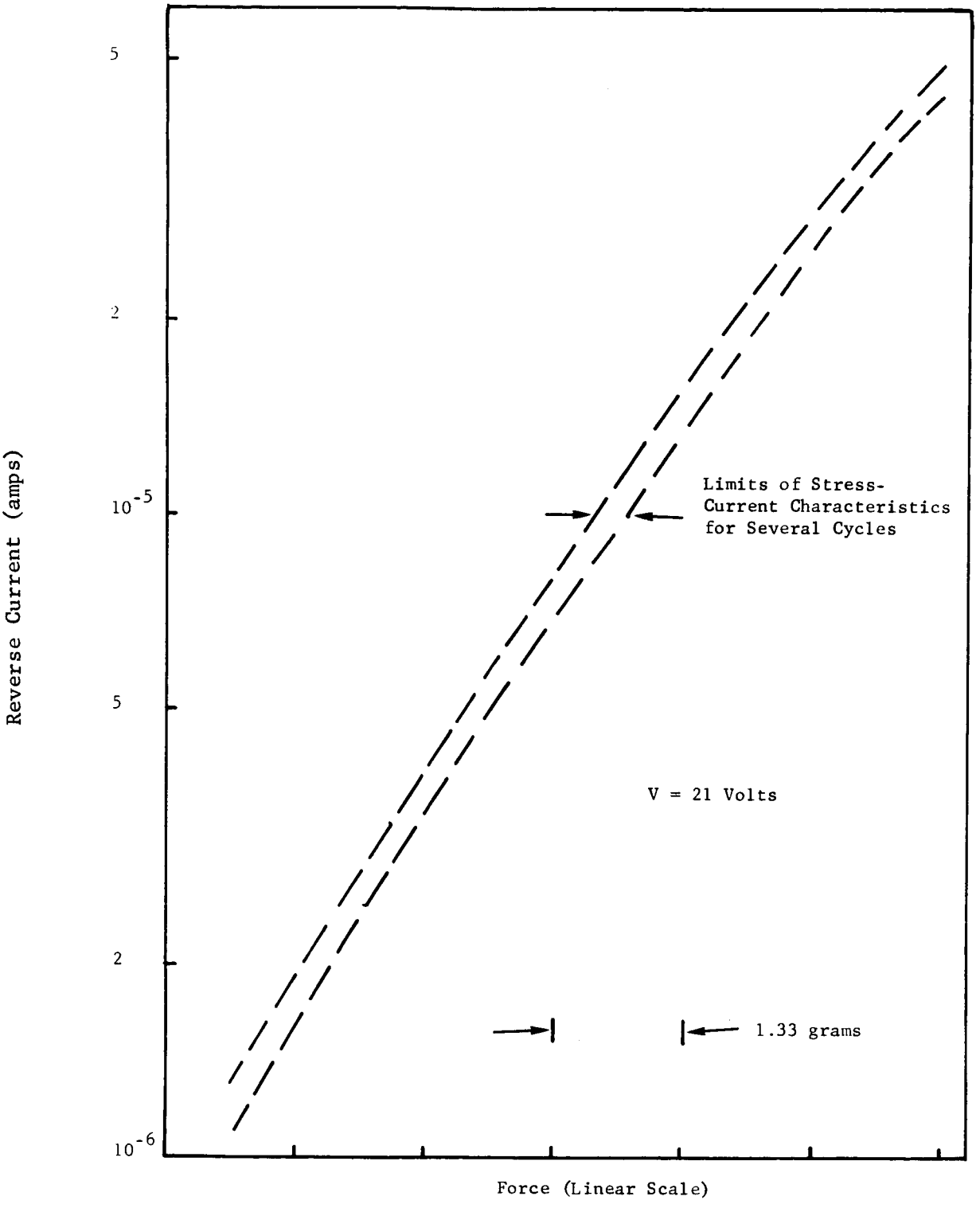

Fig. 21. Reverse Current Versus Applied Force for a Needle Sensor Stressed Against Quartz

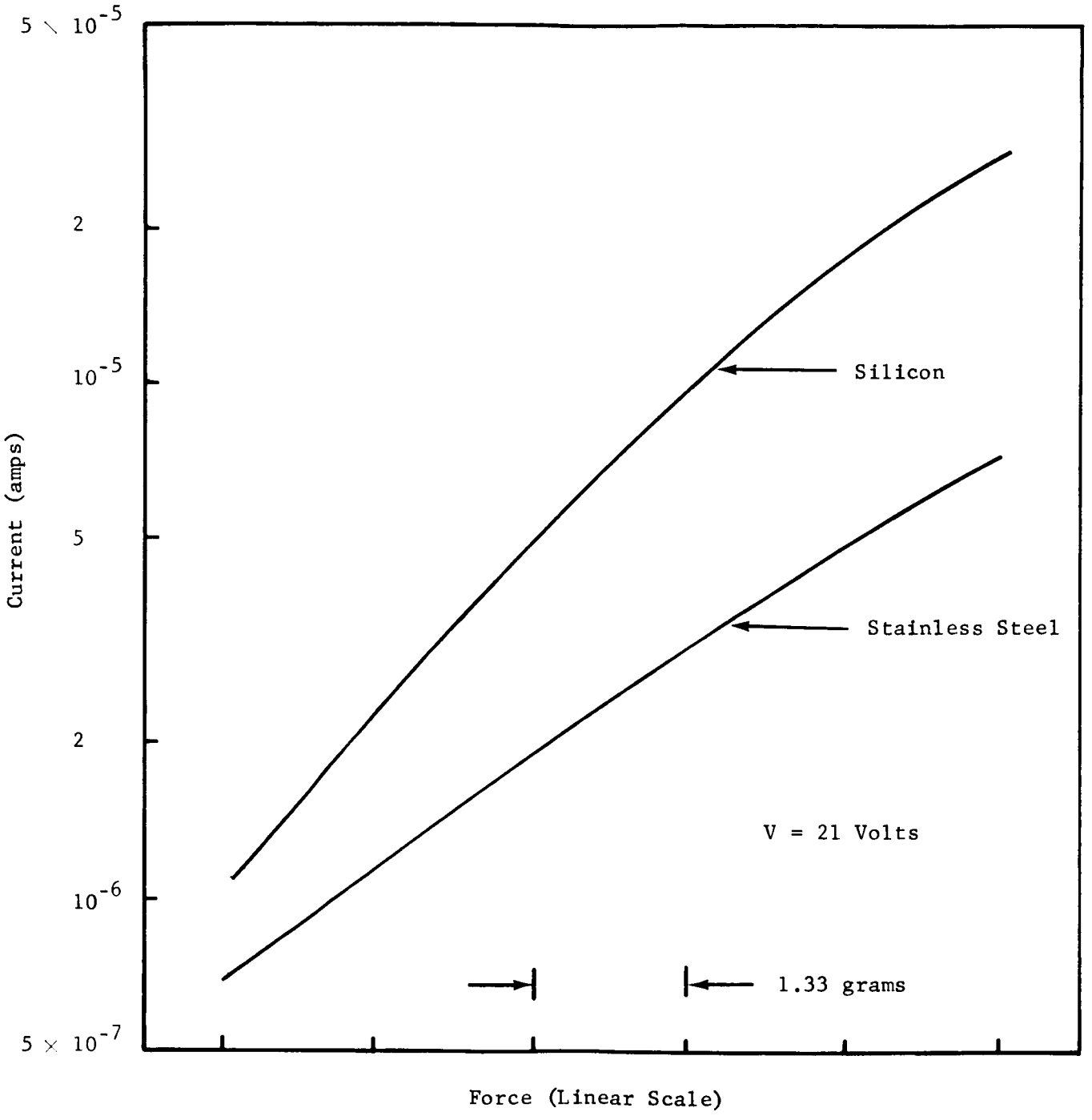

Fig. 22. Current Versus Force (Stress) for a Needle Sensor Stressed Against Stainless Steel and Silicon

case of silicon, which is "stiffer" than the stainless steel, and hysteresis tends to be less with silicon than with stainless steel. It is difficult to eliminate all mechanical hysteresis in the test apparatus used to evaluate the silicon needle sensors.

4.1.2 The Aluminized Needle Sensor

An immediate problem to be solved is the unreliable electrical contact to the tip or p-region of the silicon needle sensor. The erratic behavior and high resistance of the present contact limits the usefulness of the needle sensor at both low currents ($\approx 10^{-7}$ amps) and high currents ($\approx 10^{-4}$ amps), complicates the hysteresis problem by masking the hysteresis inherent to the needle and complicates the comparison of experimental results with theory. A solution with considerable promise is the aluminized needle in which an aluminum film is evaporated over the lower portion of the needle shank to provide the desired contact. The aluminized needle is illustrated in Fig. 23. It is expected that the aluminum film will punch-through in the high-stress, physical contact area at the needle tip, but electrical contact should be maintained around the perimeter of the oxide window. The aluminum will also reduce the residual oxide that tends to cover the needle tip at room temperature. As illustrated in Fig. 23, electrical contact to both sides of the p-n junction can be made on the needle shank, and the contacts are independent of the applied stress or area of contact with the stress plate. Numerous needles were aluminized as described, and the results of this effort are discussed in the following section. Fig. 24 is a photo-micrograph of an aluminized needle showing the aluminized shank, tip, and the nail-head

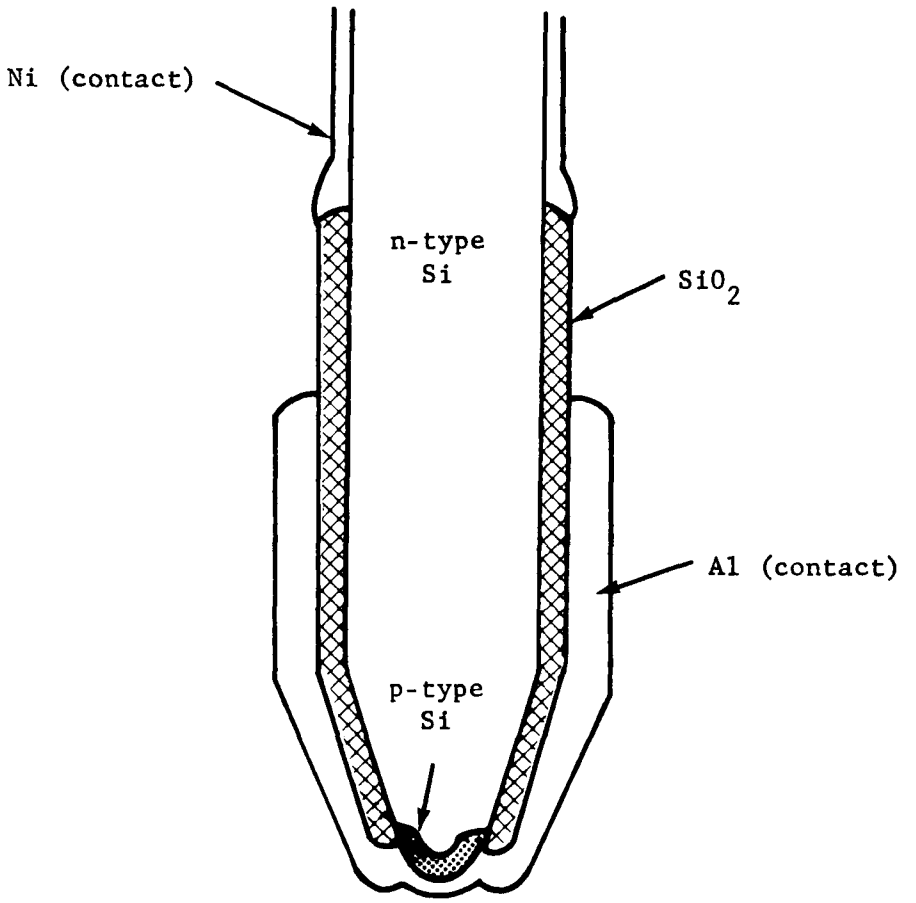

Fig. 23. The Aluminized Needle Configuration

bond to the needle shank. Fig. 25 is a close-up of the aluminized tip, and Fig. 26 is a close-up of the nail-head bond. The bonding wire is 1 mil gold.

4.1.3 The Aluminized Needle-Oxide Problem

Initial efforts to fabricate the aluminized needles have not been successful, i.e., the V-I characteristics of the aluminized needles are usually shorted or seriously degraded. The initial hypothesis was that the diffusion window was undercut during a final etch, and the

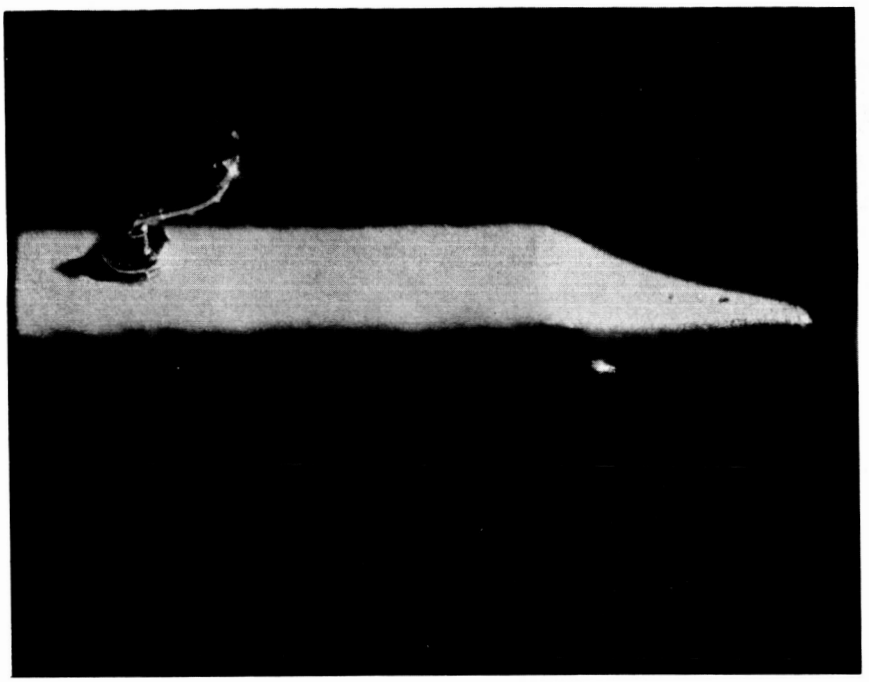

Fig. 24. A Photo-micrograph of an Aluminized Needle

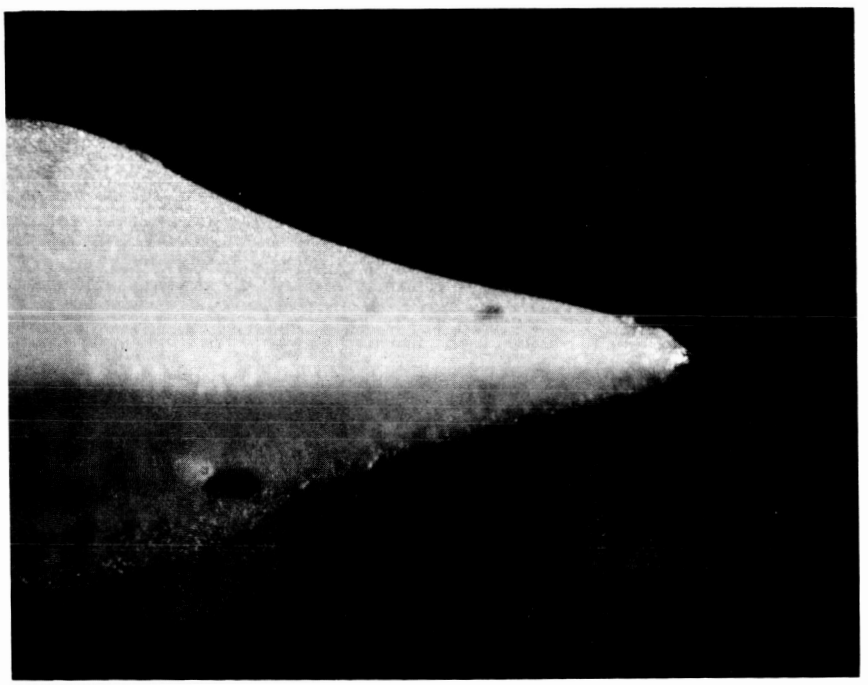

Fig. 25. A Close-up View of the Tip of the Needle in Fig. 24

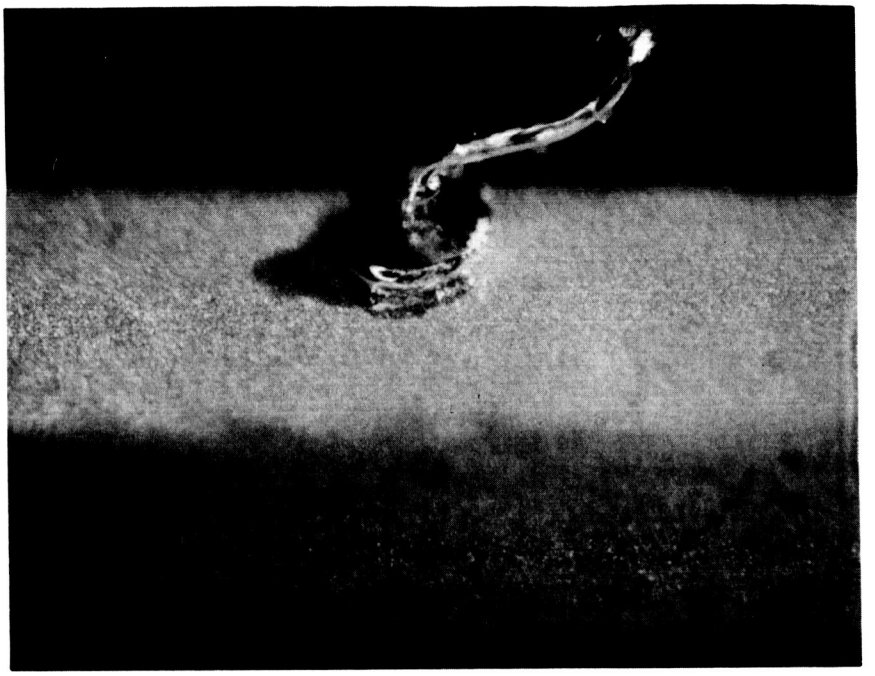

Fig. 26. A Close-up View of the Nail-head Bond in Fig. 24

aluminum film contacted both sides of the junction. Consequently, the needle fabrication procedure was modified to eliminate this possibility. Following the modified procedure, a diffusion window was first cut in the oxide at the needle tip by protecting the tip from light exposure with black wax. This procedure resulted in a larger junction area, but the size of the window could be more closely controlled. After a junction was diffused through the larger window, the protective oxide was regrown and a smaller window opened by pressing the tip against a spring-loaded black metal plate as before. This procedure provides for increased protection for the p-n junction area. However, needle sensors fabricated in this fashion and aluminized also had shorted or seriously degraded V-I characteristics.

In order to further evaluate the protective oxide, MOS structures were fabricated out of starting needle blanks. A protective oxide was grown over the entire blank, aluminum was evaporated over the oxide and selectively removed from the center. This structure is illustrated in Fig. 27. If the oxide insulates the aluminum from the underlying silicon on either end of the structure in Fig. 27, the V-I characteristics looking across the two ends will typify the MOS structure. Invariably, a low resistance, ohmic path existed between the two ends. Consequently, it was concluded that the oxide grown over the silicon blanks was porous, probably because of the rough condition of the silicon surface.

An immediate improvement in the protective oxides resulted when the entire needle surface was smoothed by etching. The etching procedure described in a preceding paragraph was followed as before except that the needle-point etch was terminated while the point was still relatively blunt. Then the needle was immersed into an agitated etch bath until the

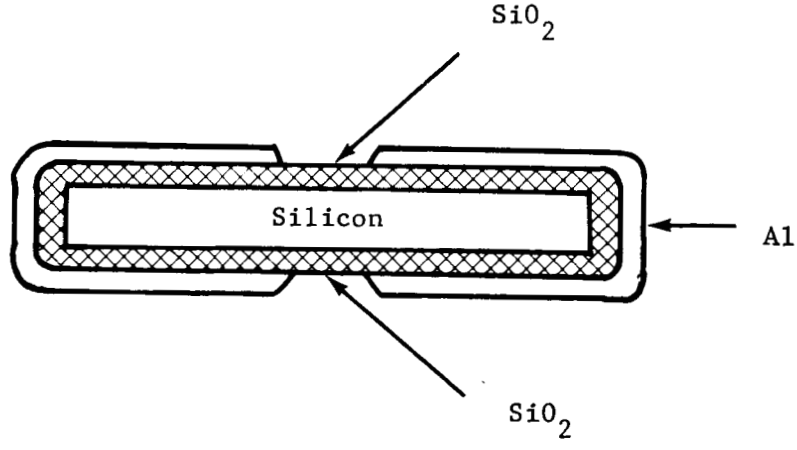

Fig. 27. An MOS Structure for Evaluating the Protective Oxides

saw damage was removed and the needle surfaces were smooth. The etch bath further sharpened the needle point and tended to round the sharp corners on the shank. The etch bath composition was the same as the etch used to sharpen the needle point, e.g., 4.5 parts HNO_3 and 1 part HF.

The silicon needles emerging from the etch bath tended to be extremely small and, consequently, difficult to handle. Subsequent needles were fabricated from blanks sawed from silicon ingots. The starting blanks cut from ingots are much larger than those cut from wafers, e.g., 45 mils on each side as compared with 20 mils on each side, and needles emerging from the etch bath are a satisfactory size. The longer etch, permissible with the ingot blanks, results in further rounding of the needle. This procedure was adopted as part of the standard needle processing procedure.

Three groups of needles were ultimately processed through the etch bath procedure; (1) blanks without a point on either end, (2) blanks with a point etched on one end, and (3) blanks with points etched on both ends. (In each case the final structure was similar to Fig. 27.) Each group was further processed as illustrated in Fig. 27, i.e., aluminum was evaporated over the entire structure and selectively removed from the center. The V-I characteristics from groups (1) and (2) tended to be the MOS characteristics expected, i.e., the yield of "good" units was greater than 50%. In group (3), most of the units had a low resistance path between the two ends of the structure, i.e., the yield of "good" devices was very small. It was concluded from these observations that the oxide was adequate over the smoothed needle surface, but tended to be inadequate at the needle point.

The hypothesis that the oxide was inadequate at the needle point was further tested by processing several small groups of needles as follows: (1) the needle blanks (from ingots) were cleaned, (2) a needle point was etched, (3) the surface was smoothed in and etch bath, and (4) a protective oxide was thermally grown over the prepared needle. The needles were then placed in a p-type diffusion furnace without purposely opening a window at the needle tip. A large percentage of the needles resulting from this experiment had p-n junction characteristics between the needle tip and the needle shank. These observations indicate that the oxide is inadequate at the needle tip, permitting unwanted impurity diffusion to occur and the evaporated aluminum film to contact the junction area and degrade the diode characteristics.

Current investigations are being directed toward improving the needle sensor technology. The basic structure illustrated in Fig. 14 can be consistently fabricated, yielding a high quality, stress-sensitive diode. Many of these have been fabricated into the pressure transducer configuration of Fig. 15. However, the sensitivity and dynamic range of these transducers are compromised by the silicon needle inadequacies. A better control over the protective oxide integrity and diffusion and contact window openings would provide an improved control over stress sensitivity, and for a low resistance contact to the needle tip, p-type region. When these are accomplished, the exponential current response to stress should extend above and below current limits. Inherent in control over the oxide window opening is the ability to fabricate more complex structures in the needle configuration, e.g., transistors and four-layer switches. Additionally, non-conductive materials can be used as stress-plate or diaphragm material.

A promising approach to improving the protective SiO_2 over the needle tip is to deposit the oxide during a pyrolysis reaction of silane gas. The needles are heated to approximately 350° C and immersed in a flow of SiH_4 and O_2. The reaction is given by [Ref. 10]

$$SiH_4(g) + 2\ O_2(g) \rightarrow SiO_2(s) + 2\ H_2O(g)^* \ . \qquad (26)$$

Several MOS structures similar to Fig. 27 with needle points on both ends have been successfully fabricated by using both a deposited and thermally grown oxide. Investigations of this oxidation technique for needle sensors is continuing.

4.2 Pressure Transducer Fabrication

Pressure transducers similar to the configuration illustrated in Fig. 15 have been fabricated and tested. This assembly is further illustrated in Fig. 28. The diaphragm (Si with an evaporated Au film) is fastened between the two sections of glass (or quartz) tubing as illustrated in the lower portion of Fig. 28, and the brass end-cap is fastened to the top glass tube as illustrated. This assembly is bonded together with an epoxy. In the upper portion, the silicon needle sensor is soldered inside a brass key machined to fit opening A in the brass end-cap. As a final step, the brass key is lowered into opening A until the needle sensor is stressed by the diaphragm. The assembly is held in this position, i.e., with the needle sensor stressed against the diaphragm until the epoxy that cements the end-cap and brass key together hardens. Electrical contact is

* g = gas, s = solid

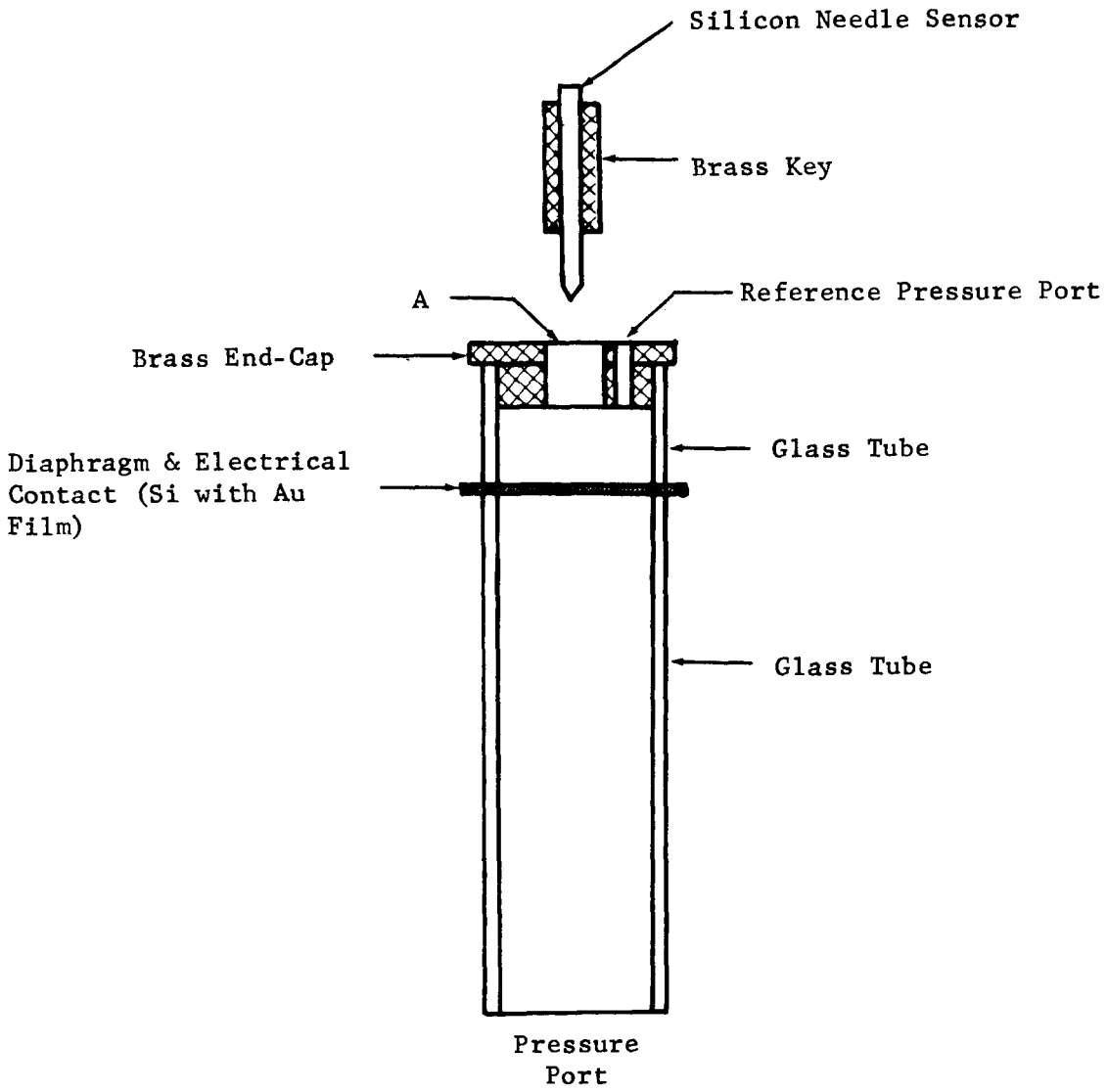

Fig. 28. An Illustration of the Silicon Needle Sensor Pressure Transducer Configuration

made across the stressed p-n junction at the silicon needle sensor top (or brass key) and the electrically conductive diaphragm (usually silicon). Any variation in pressure between the reference pressure port and the pressure port can be immediately detected in the V-I characteristics of the stressed p-n junction. Fig. 29 is a photograph showing two pressure transducers assembled as illustrated in Fig. 28. In the smaller unit of Fig. 29, the brass key was machined to fit the glass tubing and the brass end-cap eliminated. Fig. 30 is a view of a similar small transducer damaged during testing. This view is from the top of the diaphragm and needle soldered to the brass key and three reference pressure ports. The remains of the gold film that coated the silicon diaphragm are also evident in the photograph.

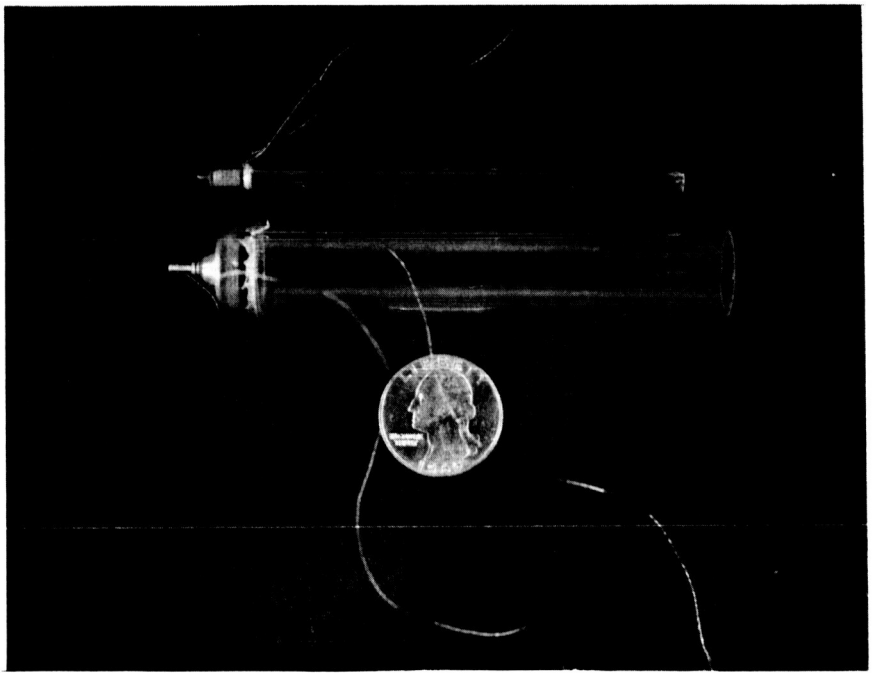

Fig. 29. A Photograph Showing Two Needle Sensor Pressure Transducers

Fig. 30. Photograph of Needle-Brass Key Assembly in the Upper Portion of a Pressure Transducer

Brass has been used in the fabrication of these pressure transducers for convenience, but it is probable that a final configuration will not contain brass. The brass key in Fig. 28, for example, can readily be replaced with glass or quartz capillary tubing with an inside diameter to accommodate the needle sensor and an outside diameter to fit the glass (or quartz) housing.

It is also probable that the epoxy bond will be eliminated in a final model of the needle sensor pressure transducer. In a few cases, silicon diaphragms have been bonded directly to glass tubing by causing the glass to melt at the glass-silicon interface. The silicon wafer is held in contact with the glass tubing and an infrared light source focused on the interface. The infrared passes through the glass to heat the silicon

which, in turn, acts as a heat source to the glass in contact with it. The glass melts at the interface and flows to adhere to the silicon. The resulting bonds are mechanically strong and leak free. Fig. 31 is a photograph showing a portion of such a bond. The glass-silicon interface is the prominent feature in the foreground.

With the basic needle structure illustrated in Fig. 14, i.e., non-aluminized, it is necessary that the diaphragm be an electrically conductive material. Most of the pressure transducers fabricated used silicon diaphragms. The few exceptions used approximately 2.5 mil quartz diaphragms coated with liquid-bright gold and an evaporated gold film. These quartz units appeared to be significantly more sensitive than comparable silicon diaphragm units, but electrical contact was not maintained long enough to collect significant data.

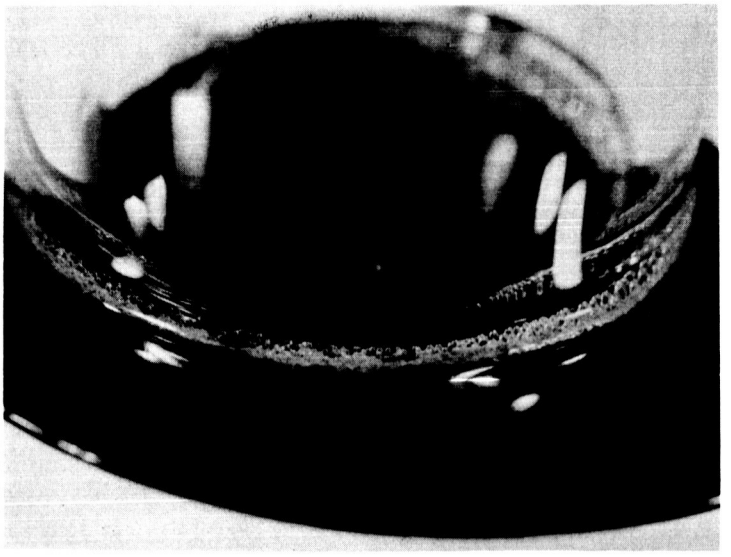

Fig. 31. Photograph of a Glass-Silicon Interface Fused with an Infrared Source.

4.2.1 Experimental Results

The voltage-current-pressure characteristics of several typical pressure transducers are illustrated in this section. The sensitivities of these units were significantly influenced, for example, by the sensitivity of the needle sensor, the diaphragm radius and the zero pressure bias. In order to simplify testing, room pressure ($\approx$ 1 atm.) was the reference pressure for all of these units. The most sensitive units fabricated, in general, tended to have electrical contact problems. Small pressure differentials reduced the contact force and the V-I characteristics became erratic. With large radius diaphragms, e.g., $r > 0.5$ in., small pressure differentials could deflect the diaphragm sufficiently to break the physical contact between the needle and diaphragm. Diaphragm diameters have ranged from approximately 0.1 in. to 1 in. Most of the units have had diameters of approximately 0.3 in.

Figs. 32 and 33 are oscillograms of forward and reverse V-I characteristics of two typical pressure transducers. Differential pressure is a parameter in these oscillograms and is labled vertically in the figures. The transducer in Fig. 32 (RTI #9) has a diaphragm diameter of approximately 0.3 in., and the transducer of Fig. 33 (RTI #8) has a diaphragm diameter of approximately 0.6 in.

The hysteresis effects in transducer No. 8, for example, are illustrated in Fig. 34. The upper oscillogram corresponds to the $\Delta P = 0$, V-I characteristics. After standing for several minutes, (1) the first exposure was made; (2) the pressure differential was increased to 30 cm H_2O, returned to zero pressure and a second exposure was immediately made; and (3) the pressure was decreased to 30 cm H_2O, returned to zero and a

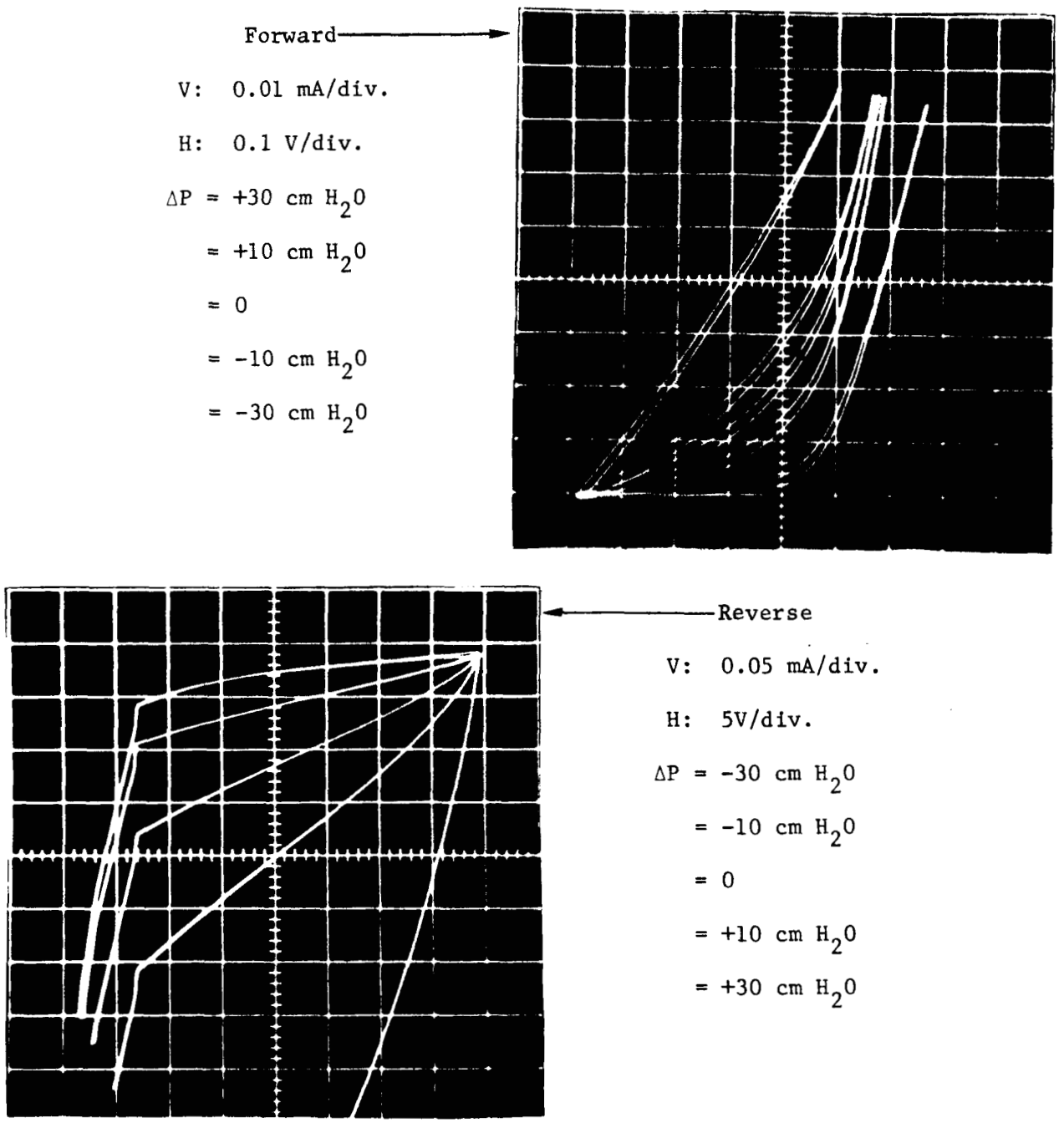

Fig. 32. Oscillograms of Forward and Reverse V-I Characteristics of a Needle Sensor Pressure Transducer; RTI #9 (1 cm $H_2O \approx 0.74$ mm Hg)

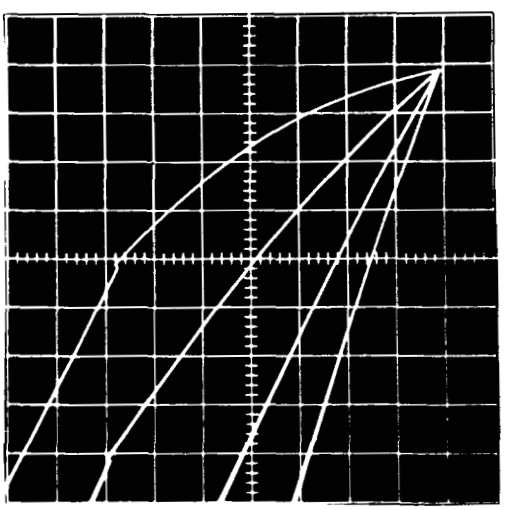

Forward →

V: 0.02 mA/div.

H: 0.05 V/div.

ΔP = 0

= -10 cm H_2O

= -20 cm H_2O

= -30 cm H_2O

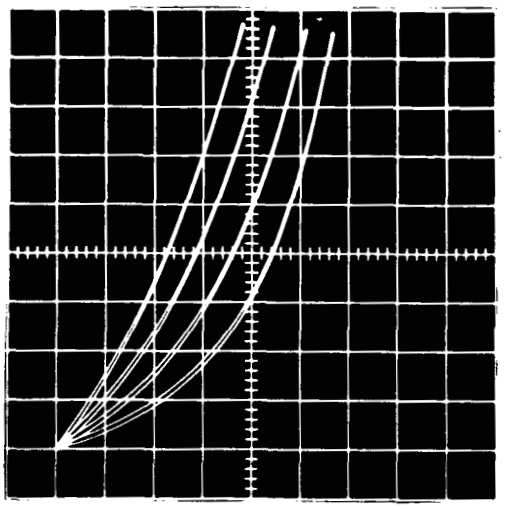

← Reverse

V: 0.2 mA/div.

H: 2 V/div.

ΔP = -30 cm H_2O

= -20 cm H_2O

= -10 cm H_2O

= 0

Fig. 33. Oscillograms of Forward and Reverse V-I Characteristics of a Pressure Transducer; RTI #8 (1 cm $H_2O \approx 0.74$ mm Hg)

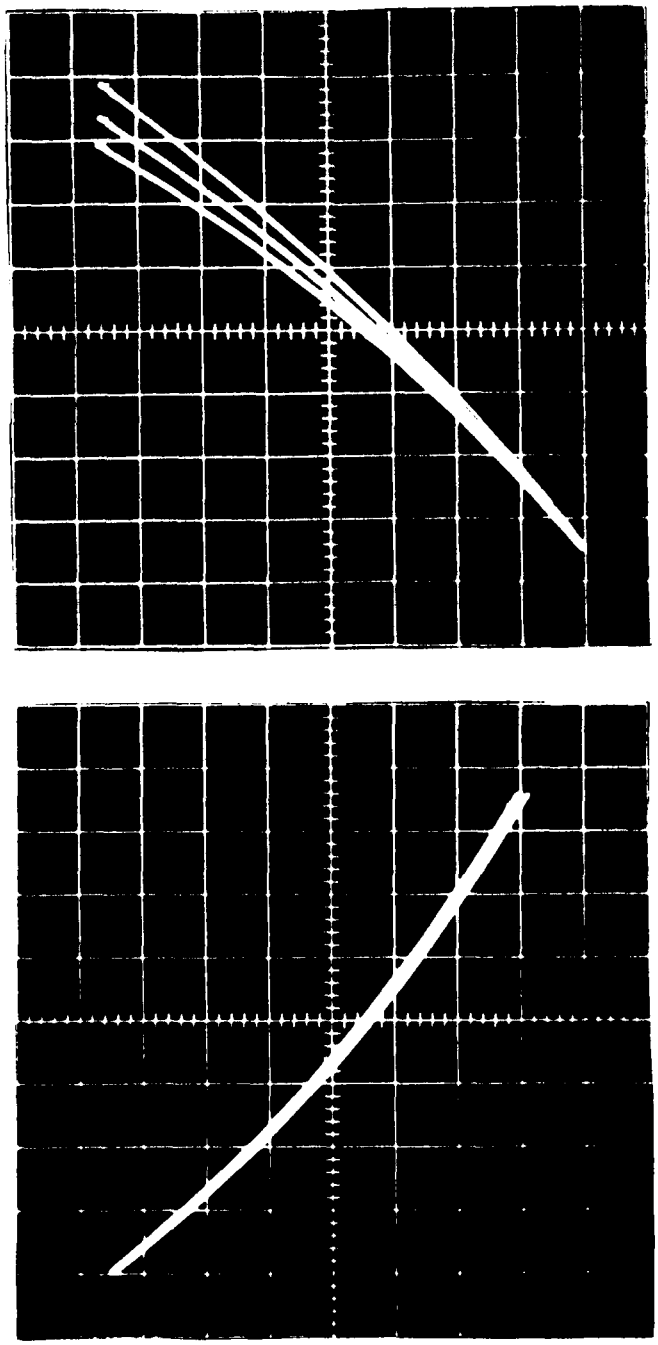

Fig. 34. An Illustration of the Hysteresis Effect (RTI #8)

V = 0.02 mA/div.

H = 0.05 V/div.

third exposure was immediately made. There was no planned delay between the exposures. In the lower oscillogram, this exact procedure was followed, but several minutes were permitted to elapse between returning the pressure differential to zero and exposing the film. This hysteresis characteristic is indicative of the creation of generation-recombination centers in the p-n junction area.

The pressure- V-I characteristics of the needle sensor pressure transducers are further illustrated in Figs. 35 and 36. Fig. 35 is a plot of the dc, V-I characteristics of a typical unit (RTI #9) for three differential pressures. This unit had a diaphragm diameter of approximately 0.3 in. In Fig. 36, the pressure-current characteristics of another typical unit (RTI #5) are illustrated. The diaphragm diameter is approximately 0.6 in. The pressure sensitivity of both these units are impressive, e.g., two orders of magnitude change in current for pressure differentials of 30 cm H_2O. The hysteresis observed in the reverse V-I-pressure characteristics varies from unit to unit and is typically 3%.

4.3 Temperature Effects

The effects of temperature on the silicon needle sensor and the pressure transducers were evaluated experimentally. The results of these experiments are summarized in this section. The needles were stressed in the test jig illustrated in Fig. 37. The "hinge" arrangement minimized the effects of dimensional changes with temperature in the jig itself and permitted stress-weights placed over the test needle to be supported primarily by the needle. The needle shank was insulated from the brass housing and stressed against a silicon chip on the cantilever beam as illustrated.

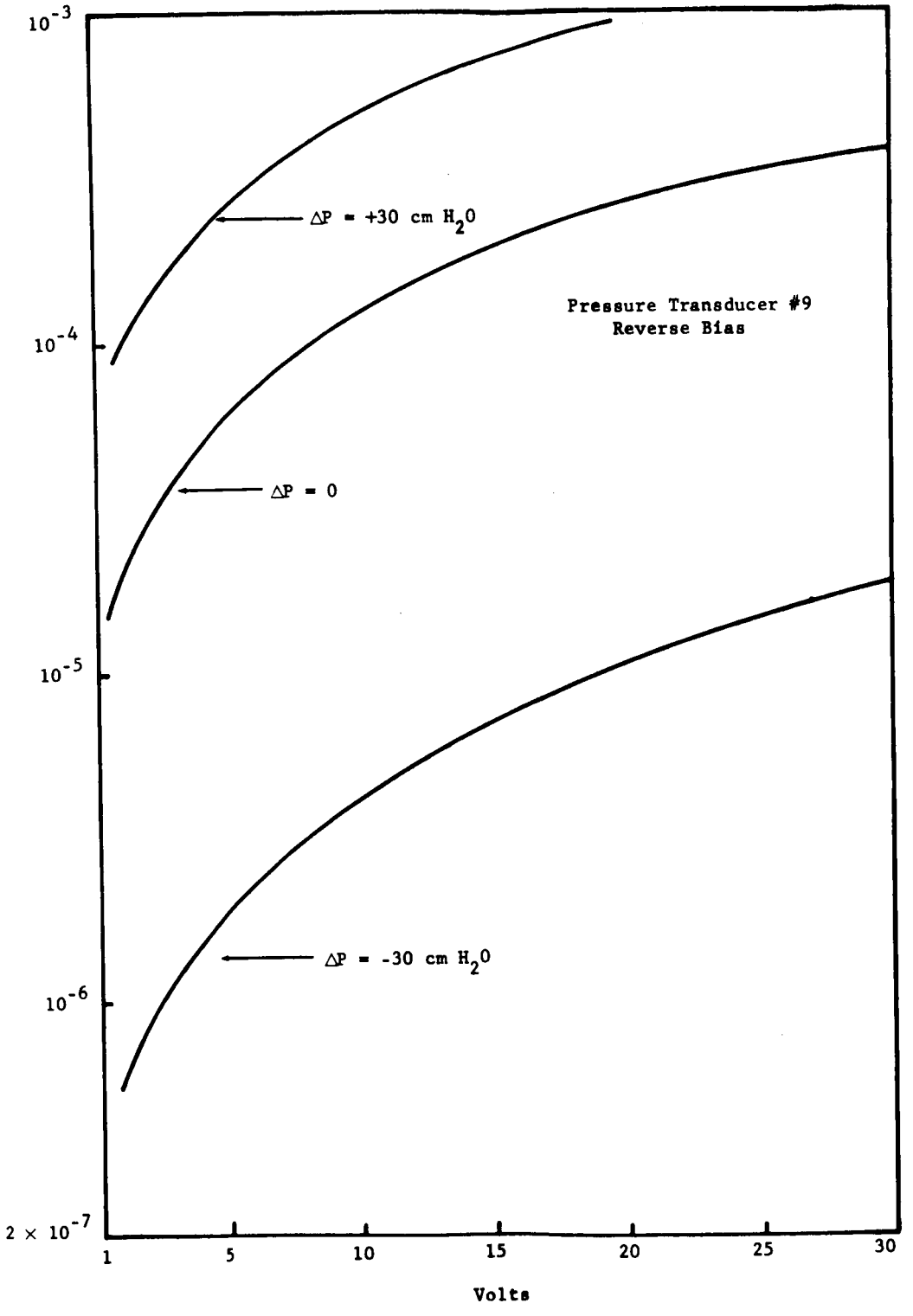

Fig. 35. DC, V-I Characteristics of Needle Sensor Pressure Transducer (RTI #9)

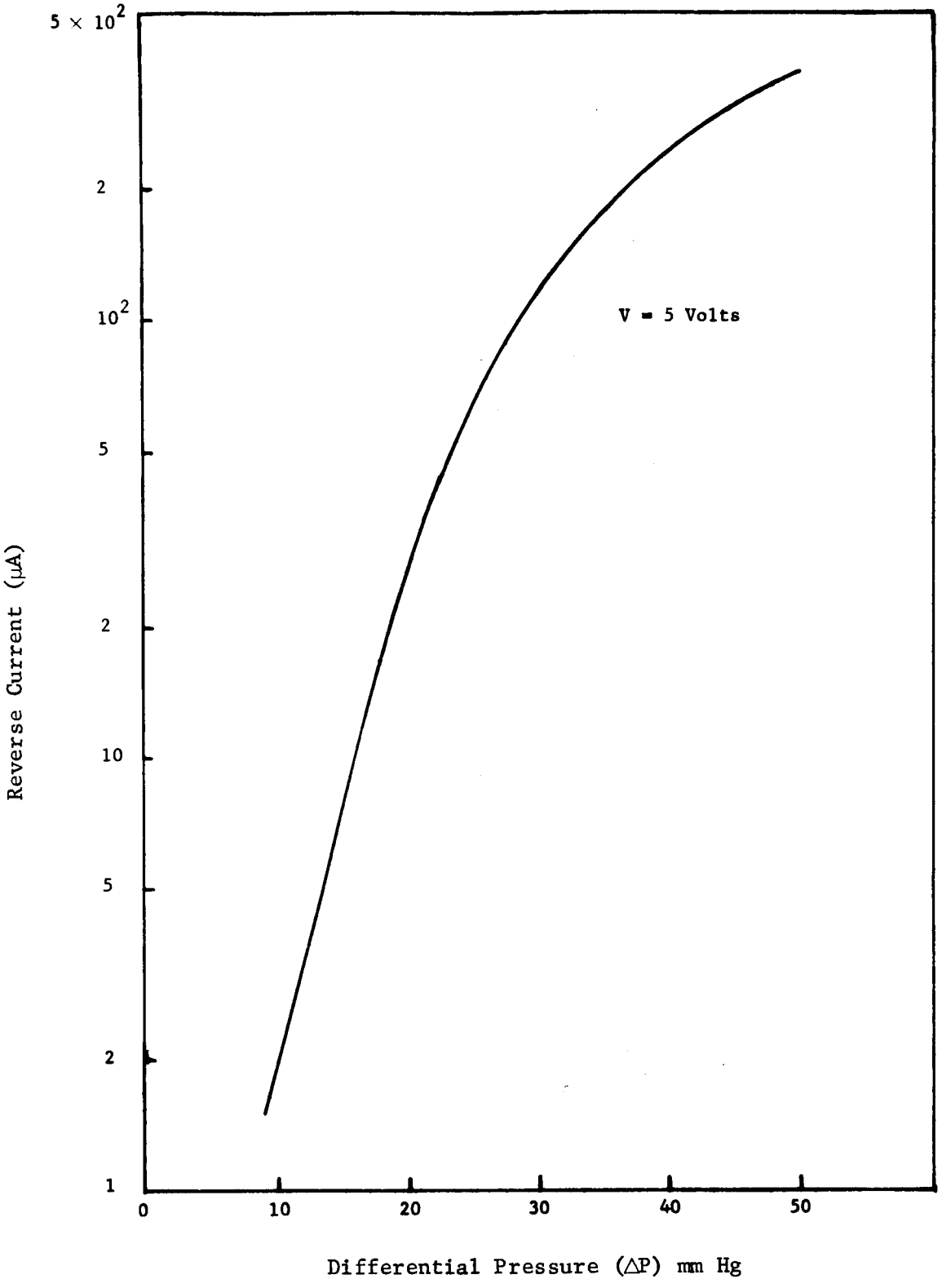

Fig. 36. Differential Pressure Versus Current in a Needle Sensor Pressure Transducer

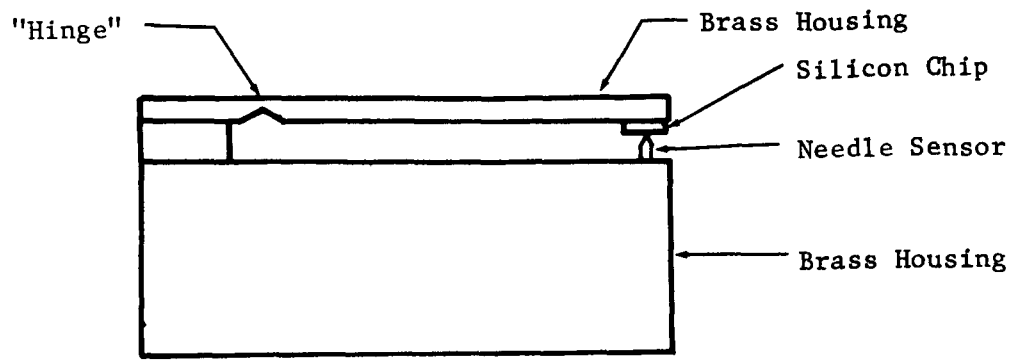

Fig. 37. Temperature Test Jig for Needle Sensor

The V-I characteristics for a typical needle changed approximately linearly from the 25° C curve to the 75° C curve in Fig. 38. The change with temperature was relatively less at high current levels, and also tended to be less at high stress levels than at low stress levels. This latter effect may be entirely due to the increased current level, however.

Several pressure transducers were also tested at various temperatures, and the results were similar to those illustrated in Fig. 38, i.e., current increased with temperature but the change was significantly less at high current levels.

4.4 Acceleration Effects

An acceleration of 150 G along an axis in the plane of the diaphragm surface of the needle sensor pressure transducer is concluded to be negligible. An acceleration along the diaphragm axis of 15 G, for example, is estimated to approximate the effect of a change in differential pressure of 1.6×10^{-3} mm Hg. (See Appendix C.)

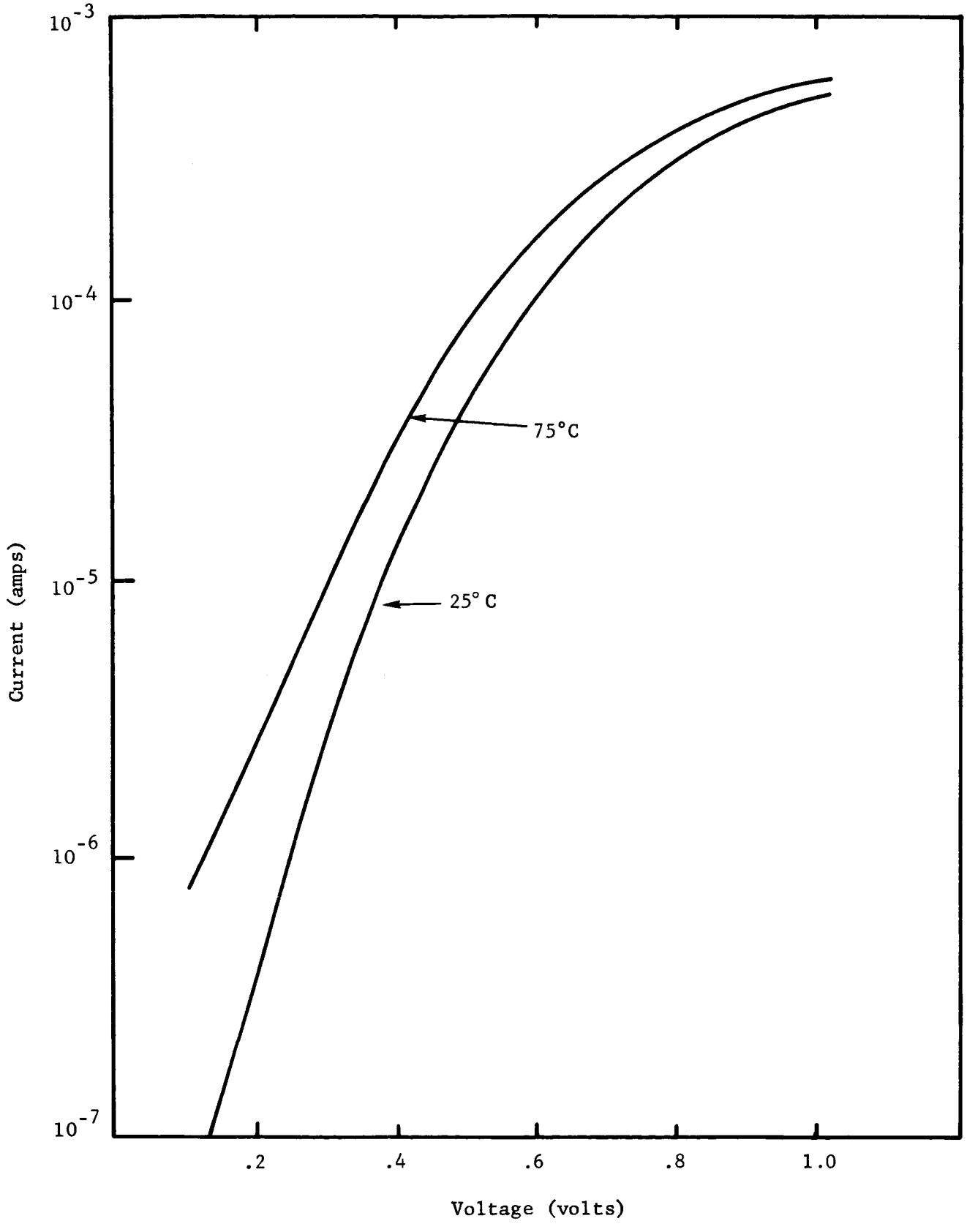

Fig. 38. Temperature Effects in a Silicon Needle Sensor

5.0 Conclusions and Recommendations

The extreme sensitivity of p-n junction electrical characteristics to stress, i.e., the piezojunction effect, make it particularly attractive as a pressure transducing mechanism. The exponential relationship between stress and p-n junction electrical characteristics predicted by piezojunction theory has been demonstrated experimentally and utilized in a pressure transducer configuration. It was concluded from an investigation of possible pressure transducer configurations that two configurations were particularly advantageous, and these were investigated in considerable detail.

A simple diaphragm configuration in which a pressure differential across a silicon diaphragm balloons the diaphragm and places the entire diaphragm material in a tensional stress is particularly attractive. This configuration has many advantages that derive from the absence of a physical contact between the p-n junction area and a stress-applying member such as an indenter point. Other advantages are derived from the ease with which an electrical contact can be made to a p-n junction anywhere on the diaphragm. These advantages cannot be overstated. There is evidence that hysteresis effects will be eliminated and that the exponential relationship between stress and the electrical characteristics of a p-n junction will extend over a much greater range. The disadvantage of the simple diaphragm configuration results from the fact that the stress achieved in the diaphragm is tensional rather than compressional, and the piezojunction effect occurs at a lower stress level for a compressional stress. Efforts to utilize the simple diaphragm were reluctantly terminated after a considerable experimental effort was invested in fabricating a simple diaphragm

transducer, and a more fruitful experimental effort was begun. It is not concluded that the simple diaphragm configuration should be abandoned in principal, however. The many advantages of this configuration make additional efforts to utilize the simple diaphragm essential as new ideas are conceived.

A second pressure transducer configuration gave excellent experimental results. The silicon needle sensor described herein has many advantages. A p-n junction can be fabricated on the needle apex that has excellent electrical characteristics and is sensitive to stress. There are no alignment problems as exist with other indenter point configurations. The junction area tends to be stressed when the needle tip is forced against a hard, smooth surface. Needle sensor fabrication is a new technology, however; and there are fabricational procedures that need to be perfected. In particular, the problem of growing or depositing a satisfactory protective oxide over the needle should be solved, and a technique for more selectively opening windows in the oxide should be solved. It is concluded that these problems have limited the sensitivity and dynamic range achieved in the experimental transducers fabricated, and it is recommended that additional effort be invested in perfecting the needle sensor technology. The optimum silicon needle sensor will be useful as the transducing element in a large family of transducers.

Other configurations require an indenter point, and these are concluded to have many disadvantages, i.e., alignment difficulties, the problem of stressing the total junction area, and the problems associated with the physical contact between the junction area and the stressing member. In the needle sensor and the indenter point configurations, this physical

contact tends to cause damage to the crystal structure, enhance generation-recombination currents and, consequently, enhance hysteresis effects.

Little effort has been invested in designing read-out circuitry to enhance the electrical output of the fabricated transducers. A direct electrical read-out is more desirable during the development stage. When the fabricated transducers are optimized, read-out circuitry will become desirable.

Efforts have not been made to optimize the range and sensitivity of the developed transducers. It was felt that the solution of more basic problems, i.e., the fabrication procedures for the needle sensors, was more important. However, sensitive pressure transducers have been fabricated, and the feasibility of a miniature solid state pressure transducer demonstrated.

LIST OF REFERENCES

1. J. J. Wortman, J. R. Hauser, and R. M. Burger, J. Appl. Phys. 35, 2122-2131, July 1964.

2. J. J. Wortman and J. R. Hauser, J. Appl. Phys. 37, 3527-3530, August 1966.

3. J. R. Hauser and J. J. Wortman, J. Appl. Phys. 37, 3884-3892, September 1966.

4. Research Triangle Institute, Feasibility Study of Piezotransistor Accelerometers, by J. J. Wortman, Contract No. NASr-222, Research Triangle Park, N. C., September 1965 (U).

5. Research Triangle Institute, Integrated Silicon Device Technology Volume V----Physical/Electrical Properties of Silicon, by R. A. Evans, Technical Documentary Report No. ASD-TDR-63-316, Vol. V, Contract AF 33(657)-10340, Durham, N. C., July 1964 (U) AD 605 558.

6. Research Triangle Institute, Research on Piezojunction Sensors, by J. J. Wortman and F. T. Wooten, Contract No. AF 33(615)-5167, Research Triangle Park, N. C., July 1967 (U).

7. R. J. Roark, Formulas for Stress and Strain, 4th Ed., McGraw-Hill Book Company, New York, New York (1965).

8. Research Triangle Institute, Feasibility Study of Piezotransistor Accelerometers, by J. J. Wortman, Contract No. NASr-222, Research Triangle Park, N. C., October 1966 (U).

9. Stow Laboratories, Preliminary Data Sheet Model PT-1, Stow, Massachusetts, September 1966.

10. Research Triangle Institute, Integrated Silicon Device Technology Volume VII----Oxidation, by R. P. Donovan, Technical Documentary Report No. ASD-TDR-63-316, Vol. VII, Contract AF 33(615)-1998, Durham, N. C., June 1965 (U) AD 618 704.

11. W. P. Mason, Physical Acoustics and the Properties of Solids (D. Van Nostrand Company, New York, 1958).

APPENDIX A

The Relationship of Stress to Strain

Strain and stress are related through Hook's generalized law,

$$[e_{ij}] = [S_{ij}]\,[\sigma_{ij}]\ , \tag{A-1}$$

where

e_{ij} = strain components,

σ_{ij} = stress components, and

S_{ij} = stiffness coefficients for the crystal.

For the case of the cubic, silicon crystal, Hook's generalized law is [Ref. 4]

$$\begin{bmatrix} e_1 \\ e_2 \\ e_3 \\ e_4 \\ e_5 \\ e_6 \end{bmatrix} = \begin{bmatrix} S_{11} & S_{12} & S_{12} & 0 & 0 & 0 \\ S_{12} & S_{11} & S_{12} & 0 & 0 & 0 \\ S_{12} & S_{12} & S_{11} & 0 & 0 & 0 \\ 0 & 0 & 0 & S_{44} & 0 & 0 \\ 0 & 0 & 0 & 0 & S_{44} & 0 \\ 0 & 0 & 0 & 0 & 0 & S_{44} \end{bmatrix} \begin{bmatrix} \sigma_1 \\ \sigma_2 \\ \sigma_3 \\ \sigma_4 \\ \sigma_5 \\ \sigma_6 \end{bmatrix} . \tag{A-2}$$

With respect to notation, e_1, e_2 and e_3 are the principal strains e_{xx}, e_{xy} and e_{yz}; e_4, e_5 and e_6 are the shear strains e_{yz}, e_{xz} and e_{xy}; and

$$e = e_1 + e_2 + e_3\ . \tag{A-3}$$

With a general stress applied to a crystal, it is possible to evaluate the principal (with respect to the crystal axes) and shear

strains. The strain components resulting from a stress are necessary for calculating $\gamma_\nu(e)$. For a hydrostatic stress of magnitude T,

$$\sigma_1 = \sigma_2 = \sigma_3 = - T \text{ , and}$$
$$\sigma_4 = \sigma_5 = \sigma_6 = 0 \text{ .} \tag{A-4}$$

From Hook's Law, the strain components are computed as

$$e_1 = e_2 = e_3 = - (S_{11} + 2 S_{12})T \text{ , and}$$
$$e_4 = e_5 = e_6 = 0 \text{ .} \tag{A-5}$$

For a uniaxial [111] stress of magnitude T,

$$\sigma_1 = \sigma_2 = \sigma_3 = \sigma_4 = \sigma_5 = \sigma_6 = - T/3 \text{ ,} \tag{A-6}$$

$$e_1 = e_2 = e_3 = - T(S_{11} + 2 S_{12})/3 \text{ , and}$$
$$e_4 = e_5 = e_6 = - T S_{44}/3 \text{ .} \tag{A-7}$$

For a uniaxial [011] stress of magnitude T,

$$\sigma_1 = 0 \text{ ,}$$
$$\sigma_2 = \sigma_3 = - T/2 \text{ ,}$$
$$\sigma_4 = - T/2 \text{ ,}$$
$$\sigma_5 = \sigma_6 = 0 \text{ ,} \tag{A-8}$$

$$e_1 = - S_{12} T \text{ ,}$$
$$e_2 = e_3 = - T(S_{11} + S_{12})/2 \text{ ,}$$
$$e_4 = - T S_{44}\sigma 2 \text{ , and}$$
$$e_5 = e_6 = 0 \text{ .} \tag{A-9}$$

For a uniaxial [100] stress of magnitude T,

$$\sigma_1 = - T ,$$
$$\sigma_2 = \sigma_3 = \sigma_4 = \sigma_5 = \sigma_6 = 0 , \tag{A-10}$$

$$e_1 = - S_{11} T ,$$
$$e_2 = e_3 = - S_{12} T , \text{ and} \tag{A-11}$$
$$e_4 = e_5 = e_6 = 0 .$$

In the preceeding equations the applied stress, T, is positive when compressional, and negative when tensional [Ref. 4].

The stiffness coefficients of silicon, S_{ij}, of Eq. (A-2) are given by Mason [Ref. 11] as follows:

$$S_{11} = 0.768 \text{ cm}^2/10^{12} \text{ dynes},$$
$$S_{12} = - 0.214 \text{ cm}^2/10^{12} \text{ dynes, and}$$
$$S_{44} = 1.26 \text{ cm}^2/10^{12} \text{ dynes} .$$

APPENDIX B

An Estimate of the Force on a Needle Located at the Center of a Diaphragm

The force on a needle located at the center of a diaphragm can be estimated by comparing two diaphragm-pressure conditions from Roark [Ref. 7]. The center deflection of a circular diaphragm, edges fixed and held, with a uniform pressure applied over its entire surface is [Ref. 7]

$$y_1 = \frac{3\,P\pi(m^2 - 1)\,a^4}{16\,\pi\,E\,m^2 t^3} \tag{B-1}$$

where

y = center deflection,

P = pressure

m = the reciprocal of Poisson's ratio,

E = Young's modulus,

a = radius of diaphragm, and

t = diaphragm thickness.

If a force, F_n, is applied at the diaphragm center, but only over a very small area compared to the diaphragm surface area, the deflection is given by [Ref. 7]

$$y_2 = \frac{3\,F_n(m^2 - 1)\,a^2}{4\,\pi\,E\,m^2 t^3} \quad . \tag{B-2}$$

These two conditions are equivalent to the needle sensor pressure transducer configuration where P is the differential pressure on the diaphragm

and F_n is the force on the needle. Since the center deflection is zero in the pressure transducer, Eqs. (B-1) and (B-2) can be equated;

$$\frac{3\,P\pi(m^2 - 1)\,a^4}{16\,\pi\,E\,m^2t^3} = \frac{3\,F_n(m^2 - 1)\,a^2}{4\,\pi\,E\,m^2t^3} \quad . \tag{B-3}$$

From (B-3),

$$F_n = \frac{P\,\pi\,a^2}{4} \quad . \tag{B-4}$$

APPENDIX C

Estimate of Acceleration Effect on Needle Sensor Pressure Transducers

The effect of acceleration along the axis of the diaphragm surface can be estimated by the force the acceleration applies to the diaphragm. This force, in turn, can be related to a pressure differential. This procedure is followed in the following example assuming a diaphragm diameter (d) of 1.5 cm ($\approx$ 0.6 in.) and a thickness (t) 6.35×10^{-3} cm ($\approx$ 2.5 mils):

$$\text{Diaphragm Volume} = \frac{\pi d^2 t}{4} = 11.2 \times 10^{-3} \text{ cm}^3 \text{ , and} \tag{C-1}$$

$$\text{Density of Silicon} \approx 2.5 \text{ gm/cm}^3 \text{ [Ref. 5] .} \tag{C-2}$$

Therefore,

$$\text{Diaphragm Mass} = 2.8 \times 10^{-2} \text{ gms .} \tag{C-3}$$

Applying Newton's law, the force required to accelerate the diaphragm mass 15 G (14.7×10^3 cm/sec^2) is

$$\begin{aligned} F &= ma \\ &= 4.1 \text{ dynes .} \end{aligned} \tag{C-4}$$

This force is applied at the diaphragm perimeter, and can therefore be considered to be balanced by a uniform force over the surface area. The surface area is

$$S = \frac{\pi d^2}{4} = 1.77 \text{ cm}^2 \text{ .} \tag{C-5}$$

Therefore, the pressure equivalent to a 15 G acceleration is

$$\Delta P = \frac{F}{S} \approx 2.3 \text{ dynes/cm}^2$$
$$\approx 1.6 \times 10^{-3} \text{ mm Hg} . \qquad \text{(C-6)}$$